Non-Radiative Resonant Wireless Energy Transfer

A Thesis Submitted to the
College of Graduate Studies and Research
in Partial Fulfillment of the Requirements
for the degree of Master of Science
in the Department of Physics & Engineering Physics
University of Saskatchewan
Saskatoon

By
Darren Hunter

Permission to Use

In presenting this thesis in partial fulfilment of the requirements for a Postgraduate degree from the University of Saskatchewan, I agree that the Libraries of this University may make it freely available for inspection. I further agree that permission for copying of this thesis in any manner, in whole or in part, for scholarly purposes may be granted by the professor or professors who supervised my thesis work or, in their absence, by the Head of the Department or the Dean of the College in which my thesis work was done. It is understood that any copying or publication or use of this thesis or parts thereof for financial gain shall not be allowed without my written permission. It is also understood that due recognition shall be given to me and to the University of Saskatchewan in any scholarly use which may be made of any material in my thesis.

Requests for permission to copy or to make other use of material in this thesis in whole or part should be addressed to:

Head of the Department of Physics & Engineering Physics

116 Science Place

University of Saskatchewan

Saskatoon, Saskatchewan

Canada

S7N 5E2

Abstract

This thesis describes a theoretical and experimental investigation of wireless energy transfer between high-Q resonant radiofrequency (RF) oscillators. A model used by Kurs *et al* [1] was recast in a form which enabled expression of the results in terms of measurable electrical quantities. This model was tested using circular resonant copper loop antennas at a frequency near 10 MHz. Accurate calculation of the mutual inductance between loops was required in order to predict the loop coupling parameters, and was carried out using a custom-written computer code.

Two resonant loop antenna RF oscillators were first used to check that the model predictions were accurate in the two-oscillator case. Based on the success of these tests, the model was extended to the case of three oscillators in two different configurations, the first having two receiving oscillators, and the second having two transmitting oscillators. Model predictions for both configurations were experimentally tested over a range of coil separations and angular inclinations. These experimental tests confirmed the model's applicability in the three-oscillator regime, with significant deviations from the model only being observed when any pair of loops was in very close proximity (i.e. when the separation of loop centers was comparable to the loop diameter). This may have been be due to either nonlinear dielectric losses (due to large amplitude RF electric fields) spoiling the Quality factors Q of the loop antenna resonators, or to increased capacitive coupling between loops at short distances (not included in the current model), or both. Further investigation would be required to definitively establish the origin of the deviation from the model at short distances, but from an engineering point of view accurate modelling of the performance in the "close loop" regime is not critical since the primary purpose of wireless power transfer is to transmit power over a reasonable distance.

Acknowledgements

I would like to thank Dr. Michael Bradley for his supervision and suggesting this project for a thesis. His guidance and support helped through many of the more challenging aspects of the project. We worked well as a team, even when he was in France and when I began working full time at the Canadian Light Source. I would also like to thank Dr. Glenn Hussey for a place to setup our experiment and for letting us use his equipment; the project would have had no traction without it. Thanks to Jan Wiid for sharing his wealth of knowledge in RF engineering.

I would also like thank the department for all of the opportunities they provided me over the time I spent here.

To Alan, who would appreciate the topic the most

Contents

List of Figures

List of Abbreviations

RF	Radio Frequency
PCB	Printed Circuit Board
ICNIRP	International Committee for Non-Ionizing Radiation Protection
IEEE	Institude of Electrical and Electronic Engineers
RWA	Rotating Wave Approximation
NMR	Nuclear Magnetic Resonance
ESR	Electron Spin Resonance
Q	Quality factor
AC	Alternating Current
MIT	Massachusetts Institute of Technology

Chapter 1

Introduction

1.1 Wireless Energy Transfer in Context

Wireless energy transfer is not a new idea, however, the possible efficient transmission of significant amounts of RF power has had a resurgence of interest. An early pioneer of wireless energy transfer was Nikola Tesla [2], before the creation of the modern electrical grid. Tesla's system used giant Tesla coils radiating energy in all directions, much like current telecommunications antennas. The major drawback of his proposal was that the energy would be transferred from one object to another through non-resonant magnetic induction, which greatly limited the range. Another problem was that Tesla coils generate excessively large fields. With these limitations combined with other limitations of the time, Tesla's idea was disregarded in favour of the electrical grid.

Another modern method for wireless energy transmission has been the use of high intensity lasers beaming energy onto photovoltaic cells (used for example by the University of Saskatchewan Space Design Team [3].) This method has disadvantages due to energy conversion inefficiencies and, more importantly, the requirement of a direct and uninterrupted line of sight. Should anything block the beam, all energy transfer is lost.

Despite the challenges inherent in wireless energy transfer, there has been a resurgence of interest in the idea [1]. This should not be unexpected as there are now a plethora of common wireless devices (eg. cellphones, laptops and other battery pow-

ered devices which require charging). Therefore, a new approach to wireless energy transfer is necessary. The subject of this thesis is a type of electromagnetic resonance which exploits the fact that if two resonant systems are strongly coupled, energy can be efficiently transferred from one to the other [1]. An added benefit is that energy is only transferred if the coupling is high. This last quality is quite useful because standard RF antennas launch electromagnetic waves with minimal directionality and therefore waste a great deal of the input energy by radiation into empty space. The final benefit of this new resonant wireless energy transfer method is that there is no line-of-sight requirement. Indeed, if a non-resonant object is between the receiver and the transmitter, there is no disruption in the energy transfer.

1.2 Inadequacy of Conventional Antennas

The new method of efficient wireless energy transfer operates in the near field regime. As elaborated in Appendix A, fields in this regime fall off rapidly with distance. This rapid falloff is compensated in the resonant approach by using resonators of very high quality factor Q. This enables the tuned receiver to extract power efficiently from the near field of the transmitting antenna without a strong directional dependence. In the absence of a tuned receiver, the system looks and behaves like a poorly optimized antenna. Thus for an antenna optimized to be a poor far-field emitter, efficient near field energy transfer to a high-Q tuned receiving antenna can be achieved.

1.3 Use of Resonant Coupling to Enhance Energy Transfer

In this system, both the transmitting and receiving resonant antennas require tuning such that the natural resonant frequencies are equal. This allows strong transmit-

ter/receiver coupling with a resulting efficient energy transfer. There are many useful analogies between this transmitter-receiver system and a coupled pair of two-level atomic systems (Appendix B). In order to transfer meaningful amounts of energy between the oscillators, the transmitting antenna must also be driven at the resonant frequency of the oscillators. This dramatically increases the amount of energy transmitted. All analyses in this document assume this form of resonant coupling and driving the antennas at their resonant frequency.

1.4 Current State of the Art

Photonics researchers at Massachusetts Institute of Technology, MIT, were the first to demonstrate in 2007 that technologically significant wireless energy transfer is possible between two resonant RF oscillators [1]. This has been followed by similar demonstrations by other groups [4, 5]. However, if this is to become a viable method of energy transmission there are other important aspects that need to be considered. For instance, what happens to the system if another receiver is introduced? Another transmitter? If there are multiple coupled oscillators then there is a need to know how the oscillators will be affected when additional oscillators are introduced. The purpose of this project is to lay the groundwork for analysis for systems with an arbitrary number of transmitters and receivers, for real-world applications.

Chapter 2

Resonantly Coupled Electromagnetic Oscillators

2.1 Coupled-Mode Theory of Electrical Oscillators

A method known as coupled-mode theory [6], widely used by photonics researchers, will be used in order to model the problem and provide a mathematical framework. It proceeds by decoupling a coupled second-order differential equation for a resonant system or circuit into two uncoupled first-order differential equations. A set of these equations, one for each oscillator can then be written with coupling terms introduced to account for the effects of mutual inductive and capacitive coupling.

2.2 Lossless Circuits

Consider an undamped parallel LC resonant circuit shown in Fig. 2.1. The voltage across the capacitor and inductor leads and the circulating current are described by the familiar equations:

$$v = L\frac{di}{dt} \tag{2.1}$$

$$i = -C\frac{dv}{dt} \tag{2.2}$$

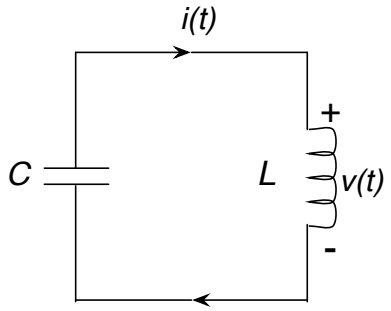

Figure 2.1: Parallel LC Resonant Circuit (undamped)

Combining these leads to the familiar second-order differential equation:

$$\frac{d^2v}{dt^2} + \omega_0^2 v = 0 \tag{2.3}$$

where ω_0 is the (angular) natural resonant frequency, defined as:

$$\omega_0 = \frac{1}{\sqrt{LC}} \tag{2.4}$$

Coupled mode theory takes a different approach. Instead of combining eqs. (2.1) and (2.2), they are decoupled by diagonalizing the system of equations. The result of this manipulation are a pair of complex variables[1] of the following form:

$$a_\pm = \sqrt{\frac{C}{2}}\left(v \pm j\sqrt{\frac{L}{C}}i\right) \tag{2.5}$$

where a_+ and a_- are usually referred to as "excitation" amplitudes. Note that they represent coherent superpositions of voltage and current and have units of $\sqrt{\text{Energy}}$.

[1] In applied physics work involving electronics, there is a dilemma regarding the choice of symbol for the imaginary number $\sqrt{-1}$. In theoretical physics and mathematics the symbol i is conventionally used. However in work involving electronic circuits the symbol i is generally reserved for AC electric current, which conflicts with this choice. The usual resolution of this dilemma in applied physics and electrical engineering is to adopt the symbol $j = \sqrt{-1}$. It was with this in mind that the convention of using $j = \sqrt{-1}$ has been adopted in this report.

Using this definition in eq. (2.3), two first-order differential equations are obtained:

$$\frac{da_+}{dt} = j\omega_0 a_+ \tag{2.6}$$

$$\frac{da_-}{dt} = -j\omega_0 a_- \tag{2.7}$$

Eqs. (2.6) and (2.7) describe the time evolution of complex amplitudes a_+ and a_-. In a waveguide regime the complex variables can be understood quite readily as the amplitudes of the voltage and current waveforms moving forward (a_+) and being reflected (a_-). For lumped circuits, eqs. (2.6) and (2.7) describe the same time evolution and only one needs to be considered; therefore a_- is ignored. When using these equations later in this thesis, the + subscript will be omitted as it is no longer necessary since a_- is no longer being considered. Our neglect of a_- is equivalent to the rotating wave approximation, RWA, frequently used in analyzing the two-level atomic systems, as well as nuclear magnetic resonance, NMR, and electron spin resonance, ESR, systems. The consequence of the RWA is that the neglected a_- solution gives rise to a shift in the true resonance frequency of the system. This shift is called the Bloch-Siegert shift [7, 8]; it is small and can be neglected under most conditions.

2.3 Lossy Circuits and the Quality Factor Q

To include the inevitable losses which occur in real systems a parallel resistor is added to the model (as shown in Fig. 2.2.) When this is done the differential equation for time-evolution of the amplitude ($a \equiv a_+$) becomes:

$$\frac{da}{dt} = j\omega_0 a - \Gamma a \tag{2.8}$$

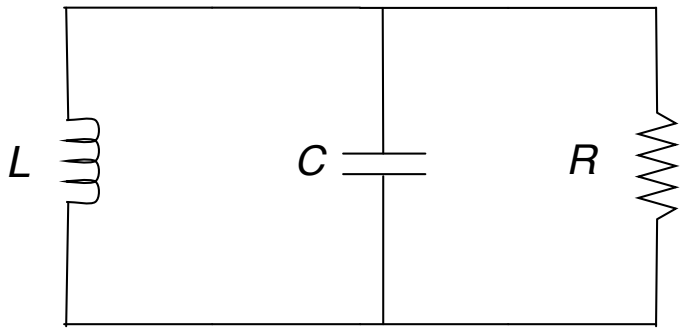

Figure 2.2: Parallel RLC Resonant Circuit ("Tank Circuit")

where $\Gamma = 1/\tau$ is the amplitude decay rate due to the added resistor and $\tau = L/R$. Note that the energy decay rate is twice this value. It is important to note that the addition of the loss to the equations in the current manner will only give an approximate solution, since the separation of the two equations was done neglecting any losses and therefore the loss is not entirely compensated for in the new set of equations. However, this ad hoc adding in loss to the model has little effect on the results of primary interest.

With the presence of loss in the system, there is a very important parameter that dictates how sharply the system can be tuned into resonance. This parameter is called the "quality factor" and is defined as,

$$Q = \frac{\omega}{2\Gamma} \tag{2.9}$$

and describes how much the losses inherent in the system affect the resonance condition. The higher the quality factor (for a given frequency), the lower the inherent losses.

Since each oscillator has its own inherent decay rate and resonant frequency, the

quality factor for each oscillator can be written as,

$$Q_i = \frac{\omega_i}{2\Gamma_i} \tag{2.10}$$

The wireless energy transfer method being analyzed in this document is effective when all resonant frequencies are tuned to be equal, i.e. when all $\omega_i = \omega_0$. In this case eq. (2.10) can be rewritten as,

$$Q_i = \frac{\omega_0}{\Gamma_i} \tag{2.11}$$

2.4 Generalization for Arbitrary Number of Oscillators

In order to extend the coupled-mode theory to multiple coupled electrical oscillators, one equation for each oscillator is written following Kurs *et al.* [1]. This gives the equations for an arbitrary number of oscillators. This set of equations includes all losses in the system and also accounts for any driving forces present. The equations are:

$$\frac{da_m(t)}{dt} = (j\omega_m - \Gamma_m)\, a_m(t) + \sum_{n \neq m} j\omega_{mn} a_n(t) + F_m(t) \tag{2.12}$$

where ω_m is the resonant frequency of the oscillator m, Γ_m is the decay rate due to losses in the oscillator (ie: $\Gamma_m = 1/\tau_m$), $F_m(t)$ is the driving force term and ω_{mn} is the coupling coefficient between the pair of oscillators m and n. The coupling coefficient is defined as [1],

$$\omega_{mn} = \frac{\omega_m M_{mn}}{2\sqrt{L_m L_n}} \tag{2.13}$$

where M_{mn} is the mutual inductance between and L_m and L_n are the self-inductances of the resonantly-tuned coils m and n. For any pair of coils $M_{mn} = M_{nm}$ (by energy

conservation [9]) and the only cases under consideration are when all oscillators have the same resonant frequency (ie: $\omega_m = \omega_n$ then $\omega_{mn} = \omega_{nm}$ for a given pair of oscillators. This result is used frequently in the following analysis. For a description of the geometries used and the formulae to calculate the mutual and self inductances, consult Appendix C.

Although not necessary to continue with the analysis, it is interesting to note that the strong coupling between the oscillators is quite similar to a resonant two-level atomic system. When an applied field drives the atomic system at its resonant frequency, the resonant frequency of the system splits. In a similar manner the coupled oscillators resonant frequency splits when the coupling between any two oscillators becomes significant. The atomic splitting is known as the Rabi frequency and is described in Appendix B to illustrate the example. The mathematical similarity between RF coupled oscillators, photonics, and atomic systems illustrate how systems in very different branches of physics can be described in a unified way.

2.5 Mapping Amplitudes to Voltages

There is one remaining aspect left to discuss; all of the analysis is done using the complex amplitudes described by eq. (2.5). However, the results obtained using these complex amplitudes need to be mapped back to voltages and currents or this method will not be useful as an engineering design tool. To begin, recall the solutions to eqs. (2.1) and (2.2),

$$v(t) = |V| \cos(\omega_0 t + \phi) \tag{2.14}$$

$$i(t) = \sqrt{\frac{C}{L}} |V| \sin(\omega_0 t + \phi) \tag{2.15}$$

where $|V|$ and ϕ are the magnitude and phase of the voltage in the LC circuit. Substituting these equations into eq. (2.5) yields the following relation for the complex

amplitudes,

$$a(t) = \sqrt{\frac{C}{2}}\left[|V|\cos(\omega_0 t + \phi) + j|V|\sin(\omega_0 t + \phi)\right] = \sqrt{\frac{C}{2}}Ve^{j\omega_0 t}. \tag{2.16}$$

This relation illustrates the dimensionality of the complex amplitudes and, consequentially, also the dimensionality of the driving force, F. Taking the square of the magnitude of eq. 2.16 yields the familiar equation for the energy stored in a capacitor,

$$|a|^2 = \frac{C}{2}|V|^2 = E \tag{2.17}$$

with E representing the energy stored in the system. Therefore, this shows that the dimensionality of the complex amplitudes is $\sqrt{\text{Energy}}$ and that the driving force has dimensionality of $\sqrt{\text{Energy}}/s$. This mapping from the complex amplitudes to real measurable quantities is used in the following chapters when analyzing the experimental data.

As a final step to map the complex amplitudes to a measurable quantity, a equation that relates the two through the potential and the inductance is desirable. Although the choice of capacitance or inductance is mathematically arbitrary, the inductance is generally not a parameter that will be varied. In order to ensure the oscillators have identical resonant frequencies, a variable capacitor will generally be used. There are also many sources of stray capacitance from nearby objects, whereas the inductance tends to be less susceptible to changes in the environment. Since the total capacitance of a system is more difficult to know accurately, the inductance is chosen for the mapping variable of choice.

To map the amplitude to the voltage, consider eq. (2.16) where the magnitude in that equation is,

$$A = \sqrt{\frac{C}{2}}V \tag{2.18}$$

with $A = |A|$ and $V = |V|$ which relates the amplitude to the potential through the

capacitance. Using the equation for the natural resonant frequency will yield the following relation for the amplitude,

$$A = \frac{V}{\omega_0 \sqrt{2L}}. \tag{2.19}$$

This relation explicitly requires the resonant frequency which is technically of no direct benefit over eq. (2.18) because the resonant frequency is susceptible to the same variations as the capacitance. However, by taking the ratio of two arbitrary oscillators tuned to resonance i.e. $\omega_m = \omega_n = \omega_0$, the following relation can be used to transform any ratio of osciallator amplitudes into a ratio of RF voltages,

$$\frac{V_m}{V_n} = \sqrt{\frac{L_m}{L_n}} \frac{A_m}{A_n} \tag{2.20}$$

where m and n are arbitrary oscillator indices. This relation is extremely useful because it illustrates a direct transformation from complex amplitudes to voltages and requires only knowledge of the self-inductance of each oscillator.

A final question remains: what about the current in the oscillator? Throughout the entire discussion thus far, the voltage was used due to the ease of a non-perturbative measurement of the voltage compared to the current. It is also common practice in electrical engineering applications of this type to measure and compare the forward transfer ratio (or more commonly, the transfer function); the ratio of the output voltage to the input voltage. Reconsidering eq. (2.17), the amplitude is related to the total energy of the system which was identical to the energy stored in the capacitor. Since the energy in the system is conserved, the total energy stored in the inductor is required to match leaving the following relation,

$$A^2 = E = \frac{C}{2} V^2 = \frac{L}{2} I^2. \tag{2.21}$$

Therefore, eq. (2.18) can be rewritten as,

$$A = \sqrt{\frac{L}{2}} I. \tag{2.22}$$

Although not used in the work in this thesis, eqs. (2.18) and (2.22) can be combined to map the voltage to the current through the following relation,

$$V = \sqrt{\frac{L}{C}} I. \tag{2.23}$$

These relations now offer the ability to convert all the relations using the complex amplitudes to measureable RF voltages.

Chapter 3

Two Oscillators

Before proceeding to multiple oscillators, it is important to verify that this formalism applies well to the case of two oscillators. Gaining confidence in the simpler system allows expansion more complex systems with more certainty. A thorough analysis ensures that the model acts as expected and discovers unexpected elements that the model does not predict, if they exist.

The chapter begins with a description of the two oscillator model. This is followed by a discussion of the equipment used for data collection, and a comparison of theory and experiment. In the later sections of the chapter, the model is reworked and expanded where further derivation is required. Comparisons between the model and experimental data are done for each aspect of the model.

3.1 Model

To solve the two-oscillator case, using eqs. (2.6) and (2.12), a set of simultaneous equations for the oscillator excitation amplitudes are set up and are written in matrix form as follows,

$$\begin{pmatrix} \dot{a_1}(t) \\ \dot{a_2}(t) \end{pmatrix} = \begin{bmatrix} j\omega_1 - \Gamma_1 & j\omega_{12} \\ j\omega_{21} & j\omega_2 - \Gamma_2 \end{bmatrix} \begin{pmatrix} a_1(t) \\ a_2(t) \end{pmatrix} + \begin{pmatrix} F_1(t) \\ F_2(t) \end{pmatrix}. \tag{3.1}$$

The amplitudes and the driving forces are phasors of the following form,

$$a_m(t) = A_m e^{j\omega t} \tag{3.2}$$

$$F_m(t) = F_m e^{j\omega t} \tag{3.3}$$

where ω is the externally selected drive frequency (i.e. the frequency of the RF generator used to excite the transmitter.). This transforms eq. (3.1) into,

$$\begin{bmatrix} j(\omega - \omega_1) + \Gamma_1 & -j\omega_{12} \\ -j\omega_{21} & j(\omega - \omega_2) + \Gamma_2 \end{bmatrix} \begin{pmatrix} A_1 \\ A_2 \end{pmatrix} = \begin{pmatrix} F_1 \\ F_2 \end{pmatrix} \tag{3.4}$$

which is the general matrix equation for the steady state amplitudes in the driven case for two oscillators.

3.2 Equipment

Three identical RF loop antenna oscillators were built from 1/4" copper pipe with a diameter of 34 cm. All three antenna loop diameters were within 0.5 cm of each other. The self-inductance for each loop (using the equation from Appendix C) was $L = 921 \pm 33$ nH. To make an RF resonant circuit, a 270 pF low-loss ceramic RF capacitor was added to each loop, such that the resonant frequency was slightly higher than 10 MHz. Optimal coupling requires identical resonant frequencies for all oscillators, therefore a small 50 pF variable tuning capacitor was added to each loop to account for any differences in the shape of the loop, error in stated values due to manufacturing uncertainty, or any other small external effects.

To measure the frequency, an HP4195A spectrum analyzer was used in conjunction with an HP41951-61001 impedance test adapter. These were connected to a non-resonant copper loop with similar physical dimensions as the resonant oscilla-

tors. This loop does not play a role in the measurement of the frequency because it is not configured as a resonant circuit and its Q-factor is spoiled by the source impedance of the spectrum analyzer. Experiments with a driven source used a Rohde & Schwarz SMB100A RF signal generator.

Three identical oscilloscopes were used to measure the voltages on the various resonant loops. They were Tektronix TDS1002 models, 2 channel digital storage scopes (50 MHz, 1GS/s.) The scope probes used were Tektronix P2200 probes (200 MHz, 10 $M\Omega$, 16 pF) used in 10x mode. Three separate oscilloscopes were used to ensure isolation between the oscillators.

Finally, to make minimally perturbative measurements of the RF voltages across the oscillator loop terminals, a high-impedance voltage divider was added in parallel to the capacitor on each loop. This minimized the Q-spoiling effect of the scope on the measurement. Two of the voltage dividers had an overall resistance of 1.22 $M\Omega$ and the other had an overall resistance of 1.04 $M\Omega$. The voltage was measured across the 100 $k\Omega$ resistor for each voltage divider network.

A photo of the entire setup is shown in Fig. 3.1.

3.3 Freqency Splitting

The first and most fundamental aspect of the coupled oscillator model is the observed splitting of the resonant frequency in strongly coupled high Q resonant systems. Solving eq. 3.4, as done in Appendix B ignoring the losses and assuming no driving terms ($F_1 = 0$ and $F_2 = 0$), yields the result that the solution for the frequency of $\omega = \omega_0 \pm \omega_{12}$. This implies the frequency splitting will be more pronounced as the coupling between the two oscillators increases.

This was tested using two oscillators aligned axially with respect to one-another. Starting at 48 cm and ending at 98 cm in 5 cm steps the frequency splitting was

Figure 3.1: Photograph of the setup used in for data collection. The third oscilloscope is out of the photo beyond the bottom left side of the photograph.

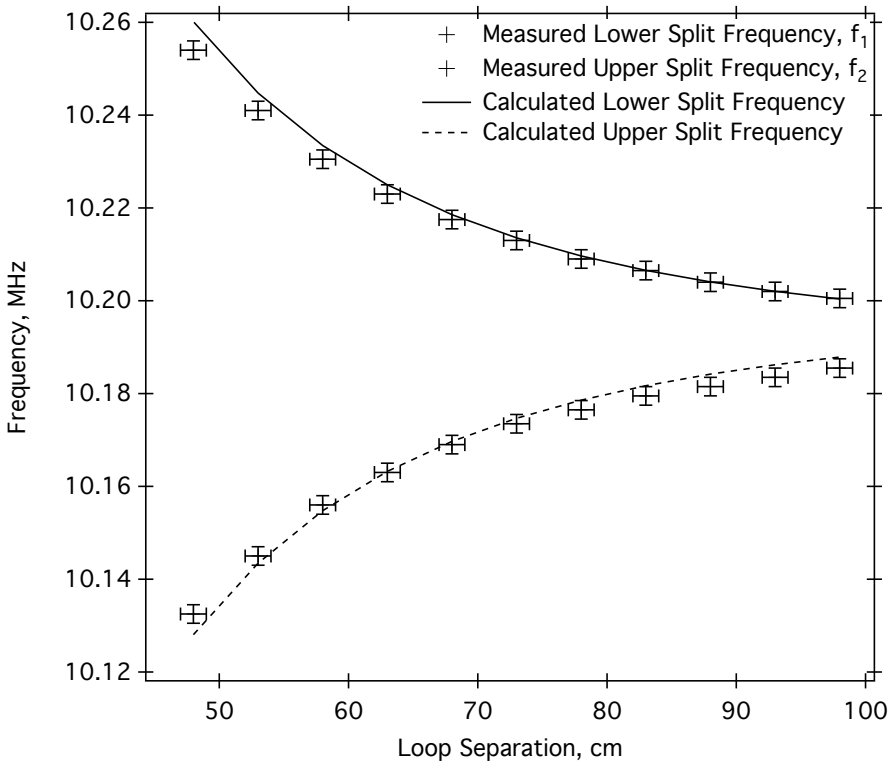

Figure 3.2: Showing the change in the splitting of the resonant frequency in a system with two highly coupled oscillators. As expected, the splitting increases as the distance between the two loops decreases. This is due to the coupling coefficient being directly proportional to the mutual inductance, which increases as the separation between the oscillators decrease.

measured with the HP4915A spectrum analyzer. The experimental results (plotted in Fig. 3.2) indeed show a splitting in the resonant frequency.

3.4 Solving for amplitudes

The key focus of this work is to ensure that the model can be used in engineering applications. Therefore, the ability to model this system using voltages and currents is a necessity. This also allows calculation of the shared energy of the system.

To start, a driving force, $F_1(t)$, is introduced to eq. 3.4 on the first oscillator, designating it as the transmitter. The other oscillator is made the receiver by F_2

being set to zero. This yields the following set of equations,

$$\begin{bmatrix} j(\omega-\omega_1)+\Gamma_1 & -j\omega_{12} \\ -j\omega_{21} & j(\omega-\omega_2)+\Gamma_2 \end{bmatrix} \begin{pmatrix} A_1 \\ A_2 \end{pmatrix} = \begin{pmatrix} F_1 \\ 0 \end{pmatrix} \tag{3.5}$$

Using Cramer's rule to solve for the amplitudes, A_1 and A_2, results in:

$$A_1 = \frac{j(\omega-\omega_2)+\Gamma_2}{[j(\omega-\omega_1)+\Gamma_1][j(\omega-\omega_2)+\Gamma_2]+\omega_{12}^2} F_1 \tag{3.6}$$

and

$$A_2 = \frac{j\omega_{12}}{[j(\omega-\omega_1)+\Gamma_1][j(\omega-\omega_2)+\Gamma_2]+\omega_{12}^2} F_1 \tag{3.7}$$

Applying the following two conditions on the general solution obtained above: the resonant oscillators condition that both oscillators have been tuned to have an identical resonant frequency ($\omega_1 = \omega_2 = \omega_0$) and"resonant drive" condition that the excitation frequency is set to match the resonant frequency of the oscillators ($\omega = \omega_0$.) Under these conditions the general solution for the amplitudes reduces to the following,

$$A_1 = \frac{\Gamma_2}{\Gamma_1\Gamma_2+\omega_{12}^2} F_1 \tag{3.8}$$

$$A_2 = \frac{j\omega_{12}}{\Gamma_1\Gamma_2+\omega_{12}^2} F_1 \tag{3.9}$$

The result qualitatively matches the two-level atomic system (Appendix B) where the receiving oscillator is exactly 90° out of phase with the transmitting oscillator. Figs. 3.3 and 3.4 demonstrate how the amplitudes vary as a function of the coupling coefficient, ω_{12}. The transmitter amplitude is initially at a maximum and then decays to zero as the coupling coefficient ω_{12} approaches infinity. The amplitude approaching zero for large coupling is interpreted as follows: if the coupling between the two systems is very high then any energy in the transmitter is immediately transferred to the receiver. The receiver amplitude starts at zero when $\omega_{12} = 0$,

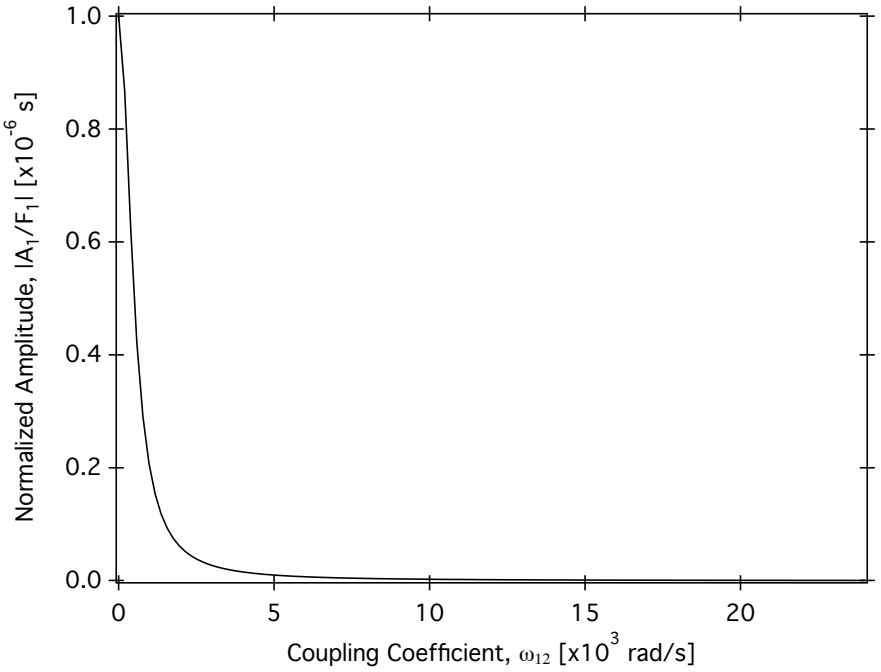

Figure 3.3: Plot of $|A_1/F|$ vs. ω_{12} illustrating how the transmitter amplitude varies with the coupling coefficient.

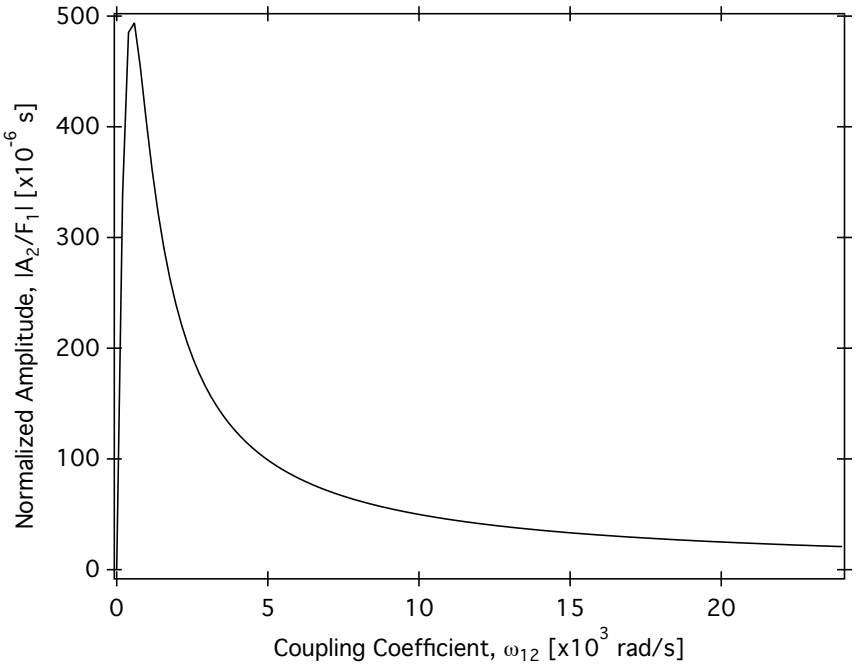

Figure 3.4: Plot of $|A_2/F|$ vs. ω_{12} illustrating how the receiver amplitudes varies with the coupling coefficient.

it then reaches a maximum and then decays. This is an important result because it implies that the amplitude on both oscillators will decrease with fixed driving force as the coupling increases. This implies that as the mutual coupling between the oscillators increases the energy being transferred back and forth between the transmitter and receiver at a rapid rate. Note that this implies that even though the transmitting oscillator is being driven, the receiving oscillator is transmitting the energy back - rapidly in the case of very high mutual coupling.

In order for these results to be more accessible to RF and power engineers, the amplitudes should be mapped to AC voltages. Eq. (2.20) yields a succinct way of relating the complex amplitudes to a ratio of AC voltages. The ratio of the receiver AC voltage to the transmitter AC voltage is called the transfer function, and it is one of the most common tools used by electrical engineers for circuit design and analysis. The ratio of A_2/A_1 is found using eqs. (3.8) and (3.9),

$$\frac{A_2}{A_1} = j\frac{\omega_{12}}{\Gamma_2} \tag{3.10}$$

Substituting eq. (3.10) into eq. (2.20) gives the following relation for the transfer function,

$$\frac{V_2}{V_1} = jQ_2\frac{M_{12}}{L_1} \tag{3.11}$$

Inspecting eq. (3.11), the receiver remains 90° out of phase, as expected. This will always true because the quality factor, mutual inductance, and the self-inductance are real quantities regardless of the system geometry. The equations are now in a more accessible form because the Q-factor, mutual inductance, and self-inductance are all known quantities in electrical engineering. All of the comparisons in future sections will be comparing the magnitudes, therefore the magnitude of the transfer function is,

$$\left|\frac{V_2}{V_1}\right| = Q_2\frac{M_{12}}{L_1}. \tag{3.12}$$

3.5 Coupling Coefficient and Mutual Inductance

Eq. 3.12 provides a means of comparing the model to measurable RF circuit quantities. For the purposes of this work, one missing piece is knowledge of the mutual inductance, M_{12}. This quantity is a function of the relative positions and orientations between the two oscillator loop antennas. In order to make any comparisons of the voltage amplitudes to the model given by eq. 3.12, an accurate calculation of the mutual inductance is required.

Eq. 2.13 can be written specifically for the system described earlier. Notationally, the 1 refers to the transmitting oscillator and 2 refers to the receiving oscillator. Recall that the inductances are identical within a margin of error. Eq. 2.13 becomes

$$\omega_{12} = \omega_0 \frac{M_{12}}{2L}. \tag{3.13}$$

with the splitting being symmetric around the resonant frequency, the coupling coefficient, written in terms of frequency, is equal to half the total frequency difference between the two peaks,

$$\omega_{12} = \frac{f_{12}}{2\pi} = \frac{\Delta f}{4\pi}. \tag{3.14}$$

Combining the two equations and solving for the mutual inductance yields,

$$M_{12} = \frac{\Delta f}{f_0} L \tag{3.15}$$

yielding a direct, unambiguous relation to compare the mutual inductance.

The measurements were performed by scanning the receiving oscillator coaxially along the axis defined by the normal to the transmitter loop plane from 48 cm to 98 cm in 5 cm steps and measuring the difference in frequency at each position. The results are shown in Fig. 3.6 which show excellent agreement, with a goodness

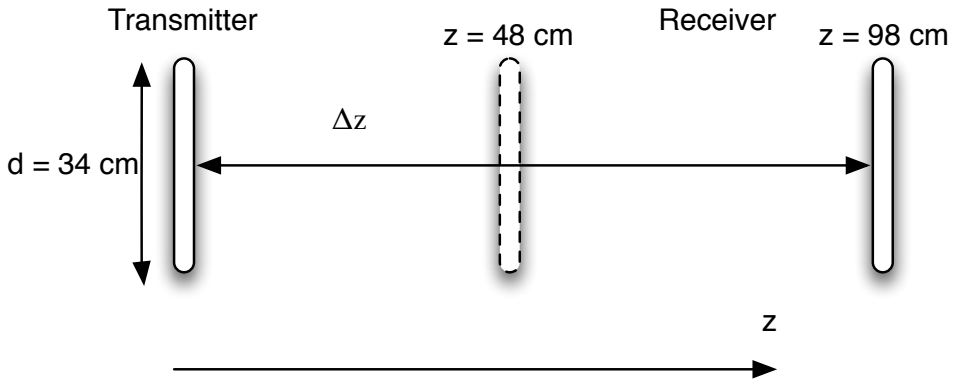

Figure 3.5: Schematic of the geometry used in the mutual inductance verification experiment. The receiver is scanned coaxially along the axis of the transmitter from 48 cm to 98 cm in 5 cm steps. The diameter of each loop is 34 cm.

of fit, χ^2_ν, of 1.36, between the calculated and experimental values. This provides great confidence when using the mutual inductance calculations in the future transfer function comparisons of the following sections.

3.6 Transfer Function

3.6.1 Introduction

The following section compares the measured transfer function to the theoretical relation from eq. 3.12. However, the mutual inductance is dependent not only on the relative position between the two circular loops, but also on the orientation of the loops, as described in Appendix C. This is an important consideration since there is no guarantee that real world applications will have coaxially aligned oscillators on the axis defined by the normal to the transmitter oscillator loop.

There are two distinct cases that will be analyzed in the following section: scanning the receiver loop coaxially along the axis defined by the transmitter and scanning a receiver laterally at a fixed axial separation from the transmitter. With the lateral

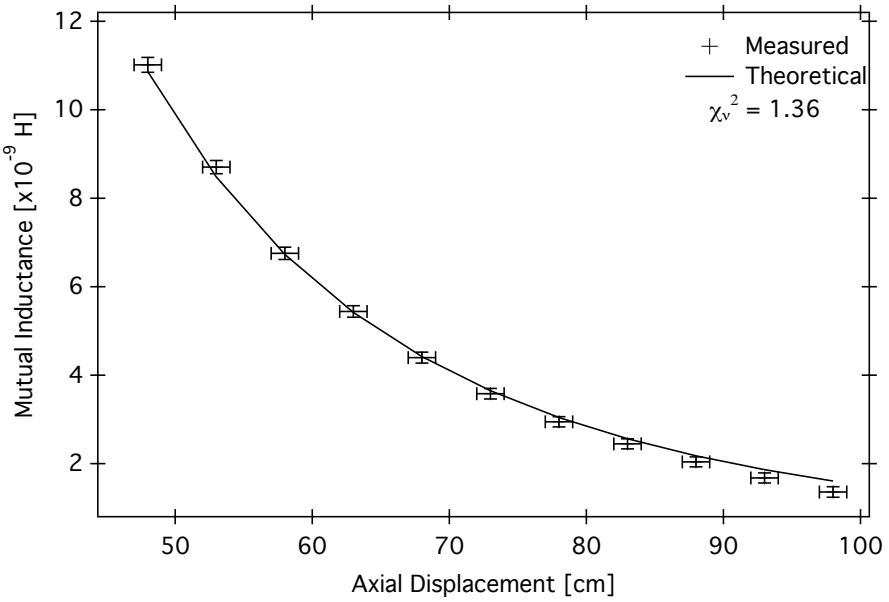

Figure 3.6: Comparison between measured and calculated mutual inductance of two circular loops based on eq. 3.15. The two curves agree very well with a $\chi^2_\nu = 1.36$.

scans, the orientation of the receiver oscillator will be investigated at the following receiver angles: 0°, 45°, and 90°.

3.6.2 Axial Geometry

This geometry is almost identical to the geometry shown in Fig. 3.5 but with different extrema. The receiving oscillator was scanned coaxially from 41 cm to 152 cm in 10 cm steps and the RF voltages on the transmitting and receiving oscillators were measured simultaneously. A schematic of the experiment geometry is shown in Fig. 3.7. The expected shape of the curve should be identical since the only parameter that is expected to change is the mutual inductance. To fit the curves, a Q-factor of 250 was required. This matches with the criterion that the system requires strong coupling between the two oscillators. Using eq. 3.12, the result in Fig. 3.8 shows that the shape of the experimental curve does not completely

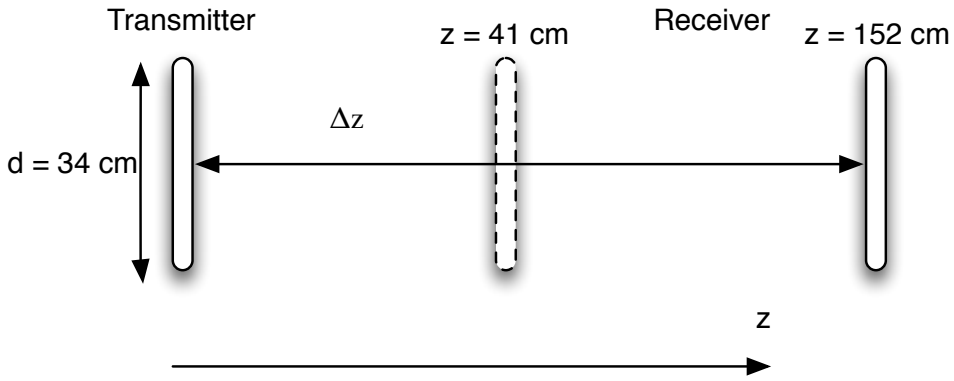

Figure 3.7: Schematic of the geometry used for this experiment. The receiver is scanned along the axis of the transmitter from 41 cm to 152 cm in 10 cm steps. The voltage on both receiving and transmitting oscillators were taken simultaneously at each step. The diameter of each loop is 34 cm.

match the theoretical prediction. As the oscillators approach each other, there is a critical distance where the magnitude begins to decrease. This deviates quite dramatically from the theoretical curve that monotonically increases as the loop separation decreases.

Looking closer at this result, there are only three quantities that can be the culprit for this change: the self-inductance of the loops, the mutual inductance between the loops, and the quality factor of the receiving loop. The self inductance is a property of the geometry of the loops - which is constant. The mutual inductance is a purely a product of the relative geometry between the two loops and has been confirmed to have the expected shape from the previous section. Specifically, the comparisons overlap and there was no discrepancy. This leaves the quality factor as the only culprit for this change in behaviour. Since the quality factor only decreases beyond some critical distance - reducing the transfer function quite dramatically - it will be referred to as"Q-spoiling". We attribute this to nonlinear losses (probably in the thin oxide layer on the copper coils) which manifest only when the surface RF electric fields are high. Such phenomenon are well known in RF engineering and could be mitigated in the furture by the use of silver-plated antenna coils.

It would be imprecise to continue discussing Q-spoiling at a critical distance. The inter-loop separation is only one parameter in determining the mutual inductance, and only meaningful because the loops were aligned coaxially. It would be more practical to discuss this junction at a critical coupling between the two oscillators. For this system, the critical coupling is $\omega_{12}/\omega_0 = 0.00212$. This number is an indirect measurement of nonlinear terms in the dielectric loss tangent of the thin (invisible) oxide layer on the surface of the copper coils.

The consequence of Q-spoiling is the reduction of the measured transfer function for all curves where the measurement takes place within the critical coupling regime (*i.e.* in regimes where the surface RF electric field exceeds a critical value, resulting in increased losses). In these circumstances, the expected transfer function will decrease, and decrease more rapidly as the effect becomes more pronounced. The rest of the measurements should agree with theoretical predictions, as the curves beyond 60 cm illustrate.

A final look at Fig. 3.8 shows excellent agreement with the theoretical predictions if the points where the Q-spoiling is ignored. The goodness of fit, χ^2_ν, ia 0.03 implying that the experiment is overestimating the errors in the model. Unfortunately, the voltage measurements at large distances were nearing the measurement limits of the oscilloscopes.

3.6.3 Lateral Geometry - Receiver Orientation 0°

The first of the lateral receiver experiments will have the receiving oscillator at an angle of 0°. The receiving oscillator is axially separated from the transmitting oscillator at a distance of 61 cm as shown in Fig. 3.9. The receiver is scanned from -76 cm to 76 cm in 10 cm steps at a constant axial separation from the transmitter.

The results are found in Fig. 3.10. This plot has the same characteristics as those found in Fig. 3.8 where the theoretical curves match very well for the majority of

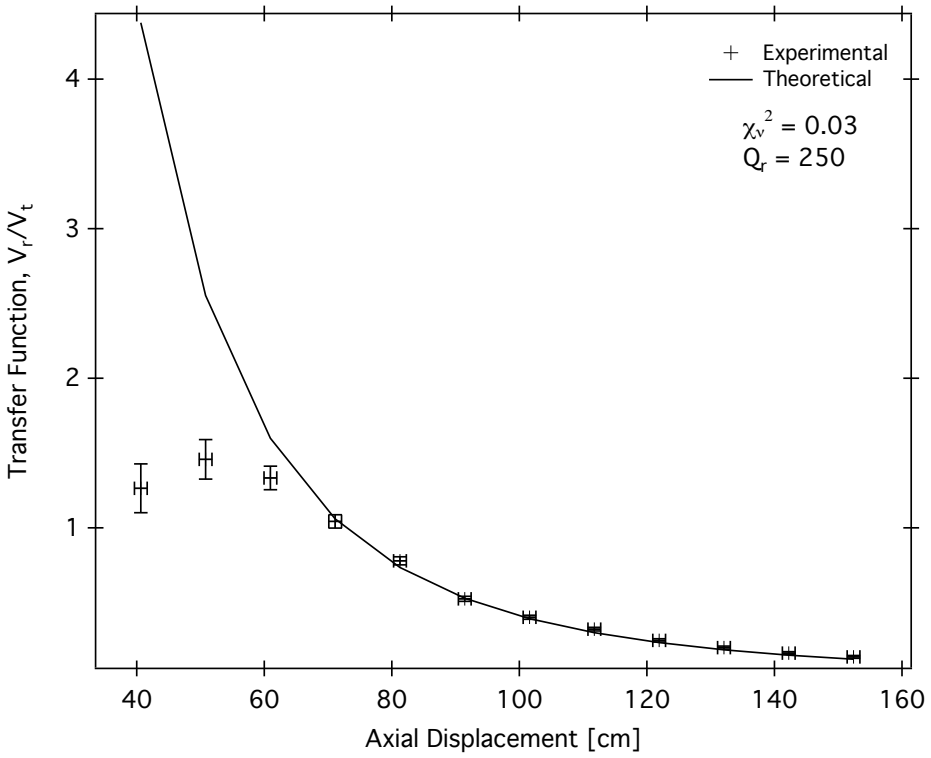

Figure 3.8: Comparison between measured and calculated transfer function of two axial aligned oscillators based on eq. 3.12. The plot exhibits Q-spoiling as the two oscillators begin to get close to each other. Ignoring the first three points, the curves agree with a $\chi^2_\nu = 0.03$.

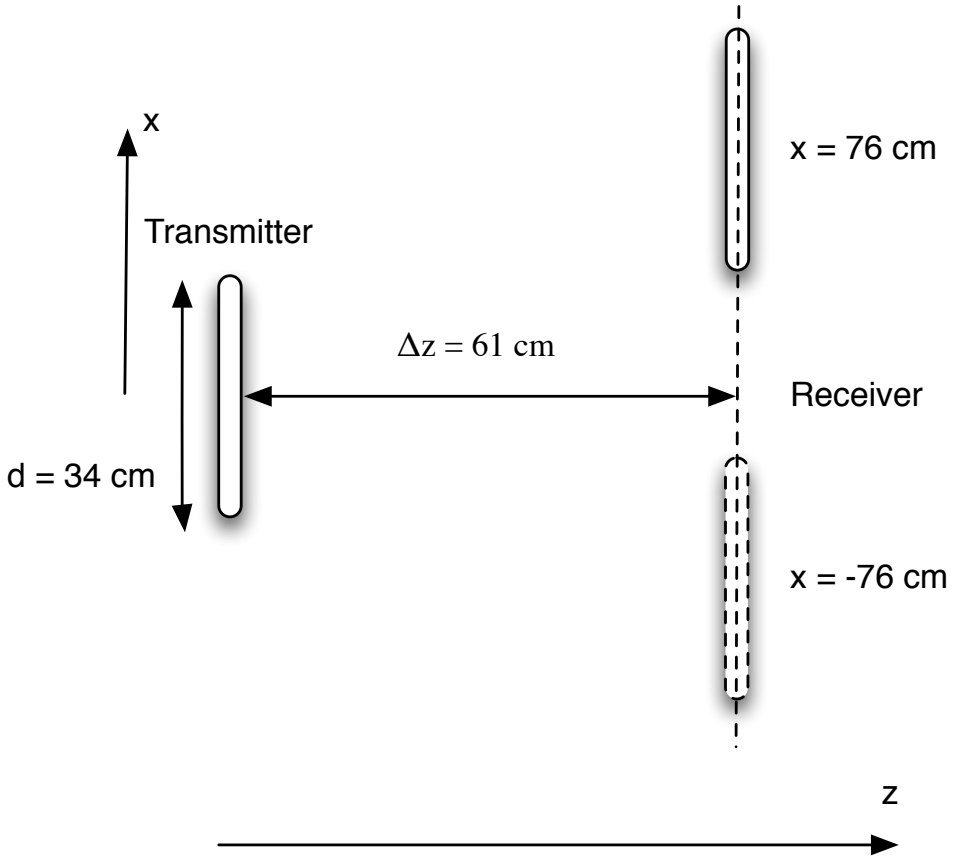

Figure 3.9: Schematic of the geometry used for this experiment. The receiver is scanned laterally from -76 cm to 76 cm in 10 cm steps at a constant axial separation of 61 cm from the transmitter. The diameter of each loop is 34 cm.

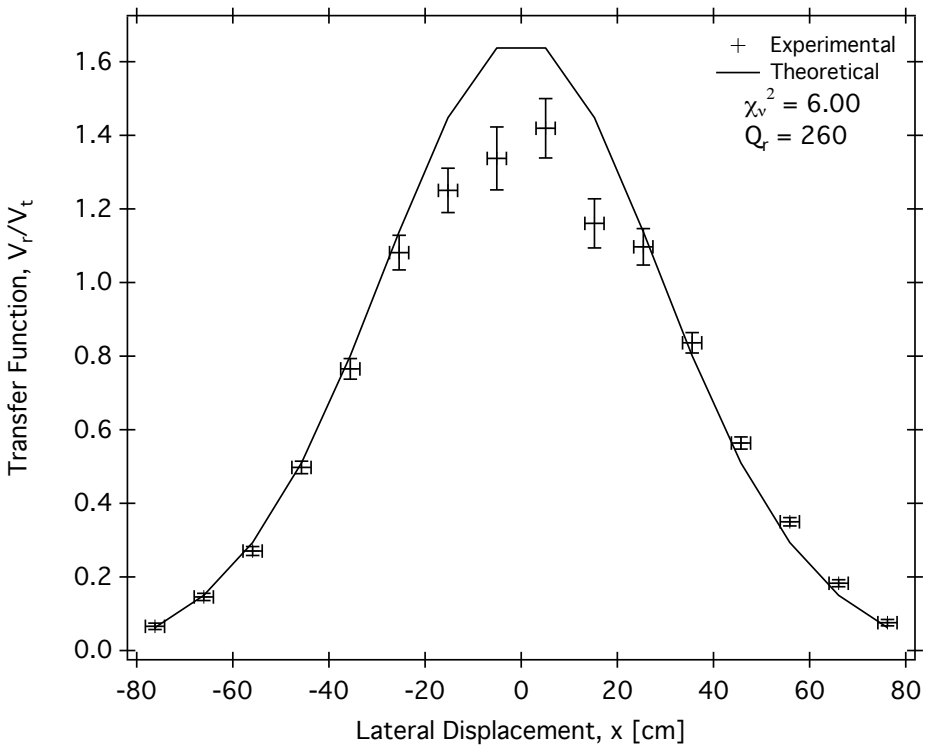

Figure 3.10: Comparison between measured measured and calculated transfer function of two oscillators with the receiver oscillator scanned laterally from -76 cm to 76 cm in 10 cm steps at a constant axial separation of 61 cm. The orientation of the receiver is at $\theta = 0°$. No points were removed from the goodness of fit calculation with a result of $\chi^2_\nu = 6.00$. χ^2_ν was high due to the middle four points affected by Q-spoiling.

points, but the middle four are all lower than the expected result. This is another example of Q-spoiling since the four of the middle points are within the critical coupling regime, where the surface RF electric field was large enough to cause nonlinear dielectric losses and spoil the Q. Since the effect of the spoiling is still somewhat small, the χ^2_ν was only 6.00 when including all the points; showing excellent agreement for all points with no Q-spoiling. To fit the curve, a Q-factor of 260 was used - matching closely to the Q-factor used for the axial scan from the previous section.

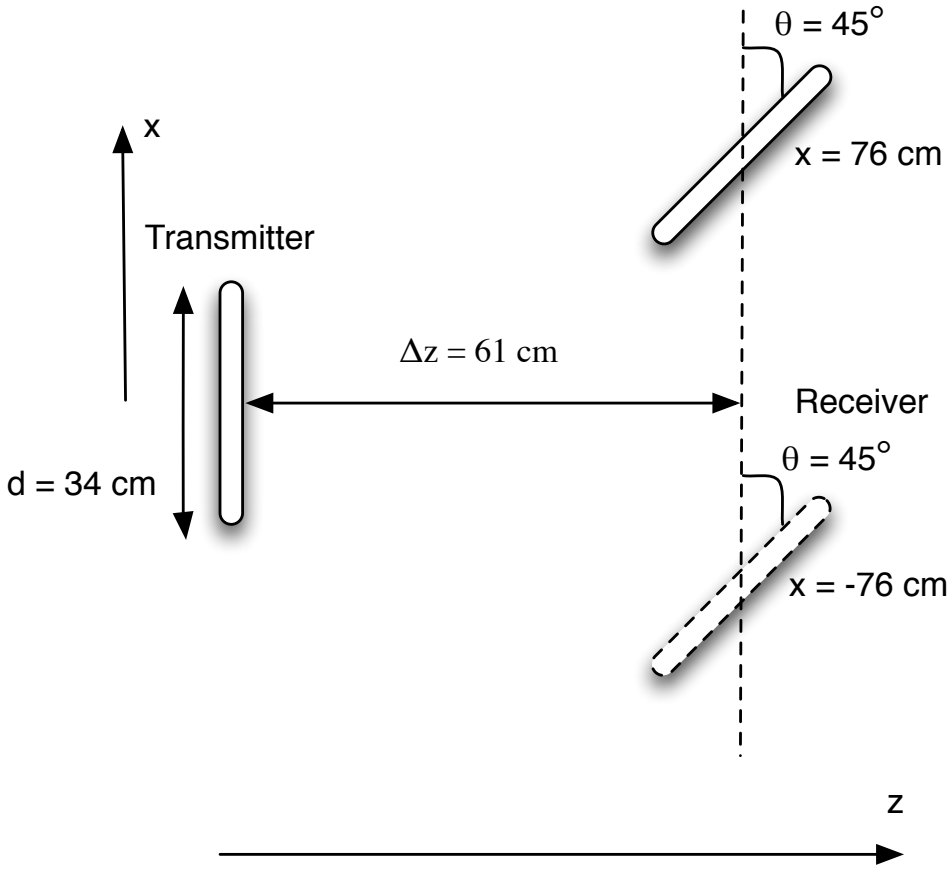

Figure 3.11: Schematic of the geometry used for this experiment. The orientation of the receiver is at $\theta = 45°$. The receiver is scanned laterally from -76 cm to 76 cm in 10 cm steps at a constant axial separation of 61 cm from the transmitter. The diameter of each loop is 34 cm.

3.6.4 Lateral Geometry - Receiver Orientation $45°$

The second of the lateral receiver experiments has the receiving oscillator at an angle of 45°. The rest of the setup is identical to the 0° setup as can be seen in Fig. 3.12.

The results of this scan are found in Fig. 3.12. Instead of being symmetric around the origin, points have been shifted to the positive side of the x-axis. This is consistent with the fact that the highest coupling between the two oscillators is not centred around the origin when the loops are not parallel. It can be seen that there is some qualitative agreement between the two plots, however, the plot exhibits

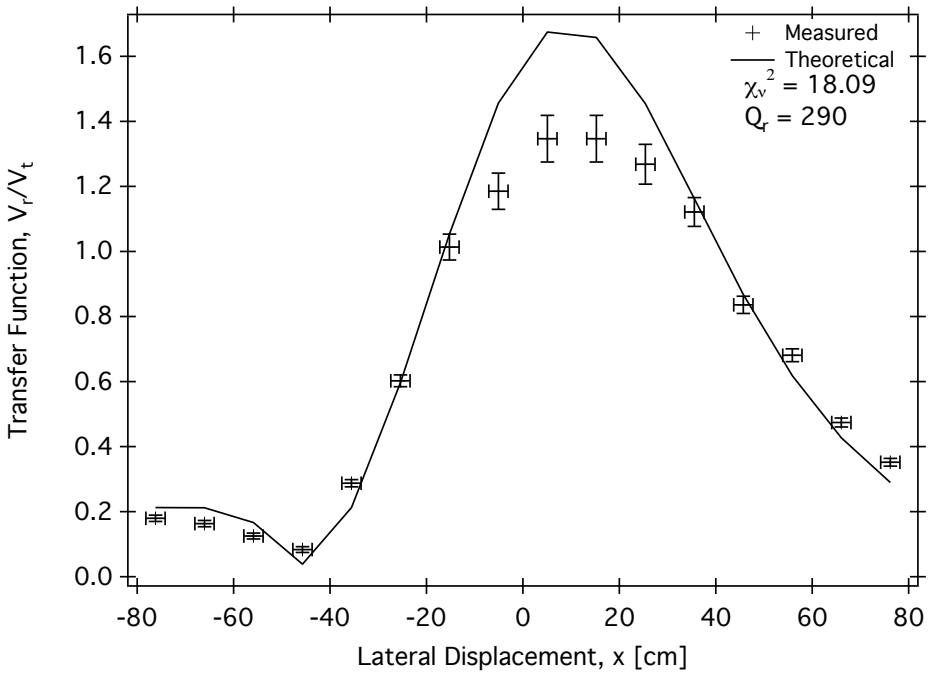

Figure 3.12: Comparison between measured and calculated transfer function of two oscillators with the receiver oscillator scanned laterally from -76 cm to 76 cm in 10 cm steps at a constant axial separation of 61 cm. The orientation of the receiver is at $\theta = 45°$. No points were removed from the goodness of fit calculation with a result of $\chi^2_\nu = 18.09$.

Q-spoiling and has a high χ^2_ν. The qualitative agreement is encouraging, but there are several reasons why this curve quantitatively fits very poorly when compared to the results seen in all of the previous sections. First, as with the curves in Fig. 3.10, there is Q-spoiling due to nonlinear losses. Second, due to the physical nature of the experimental setup, it is extremely difficult to maintain a constant angle for the receiver loop. With the large size of the two loops, when they are either parallel or perpendicular to each other, a grid marked on the floor was used to help maintain the orientation of the loops. Therefore the angle of the receiving loop could be markedly different between every point. With a setup that offered better angular precision, the quantitative agreement between the two curves would be better.

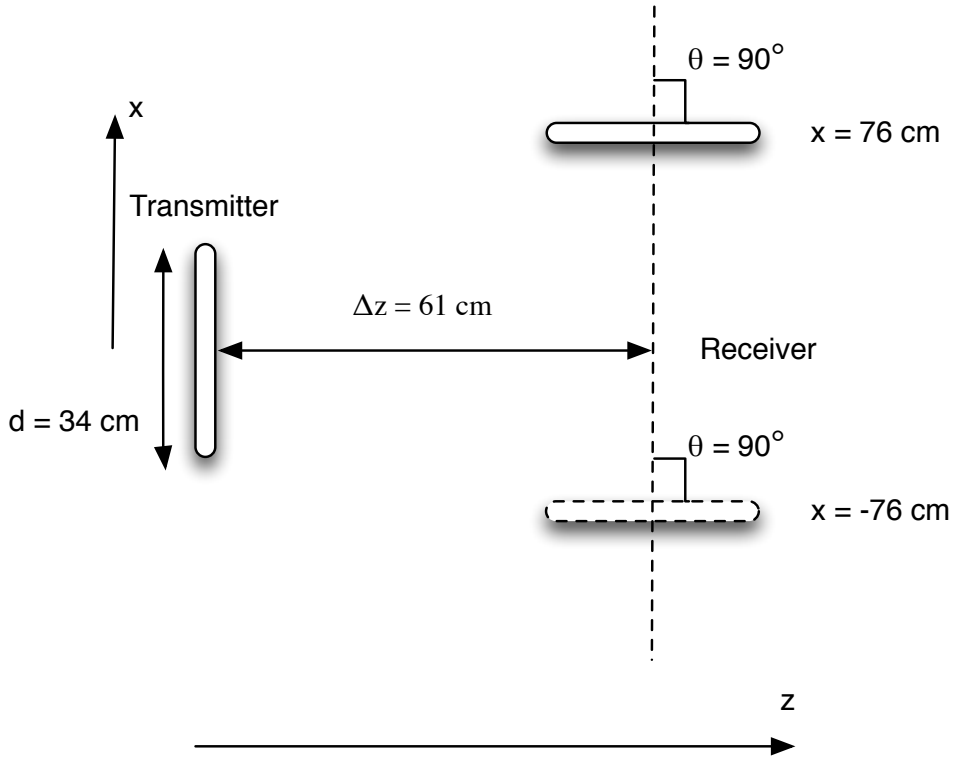

Figure 3.13: Schematic of the geometry used for this experiment. The orientation of the receiver is at $\theta = 90°$. The receiver is scanned laterally from -76 cm to 76 cm in 10 cm steps at a constant axial separation of 61 cm from the transmitter. The diameter of each loop is 34 cm.

3.6.5 Lateral Geometry - Receiver Orientation $90°$

The last of the lateral receiver experiments has the receiving oscillator at an angle of 90°. The rest of the setup is identical to the 0° setup as can be seen in Fig. 3.14.

The results of this scan are found in Fig. 3.14. The agreement between the experimental and theoretical curves is good with a χ^2_ν of 3.11. It can be seen that the last two points on the positive side of the axis begin to drift away from the expected curves. This is due to the same effect that the angular precision of the loops was difficult to keep constant throughout the entirety of the scan. However, only the last two points fell victim to this in a meaningful way. Due to this, the point at 76 cm was removed from the χ^2_ν calculation. The point at 5 cm was also removed

from the goodness of fit calculation because χ^2_ν does not take into account the error in the independent axis. Since the slope at that point was very large, its relative error was very large because the theoretical position for that point is many standard deviations from from the experimental point. Therefore, it was unnecessarily adding bias to the goodness of fit.

It is important to note that none of the experimental points in this plot were affected by Q-spoiling. This is because none of the points ever had a coupling coefficient large enough for the Q-spoiling to take effect, as seen in Figs. 3.8, 3.10, and 3.12. This adds validity to the notion that this effect is driven by a critical coupling (and corresponding critical electric field) rather than a relative position of any two oscillators. It also further validates that the model appears to match well with experiment when Q-spoiling is not in effect.

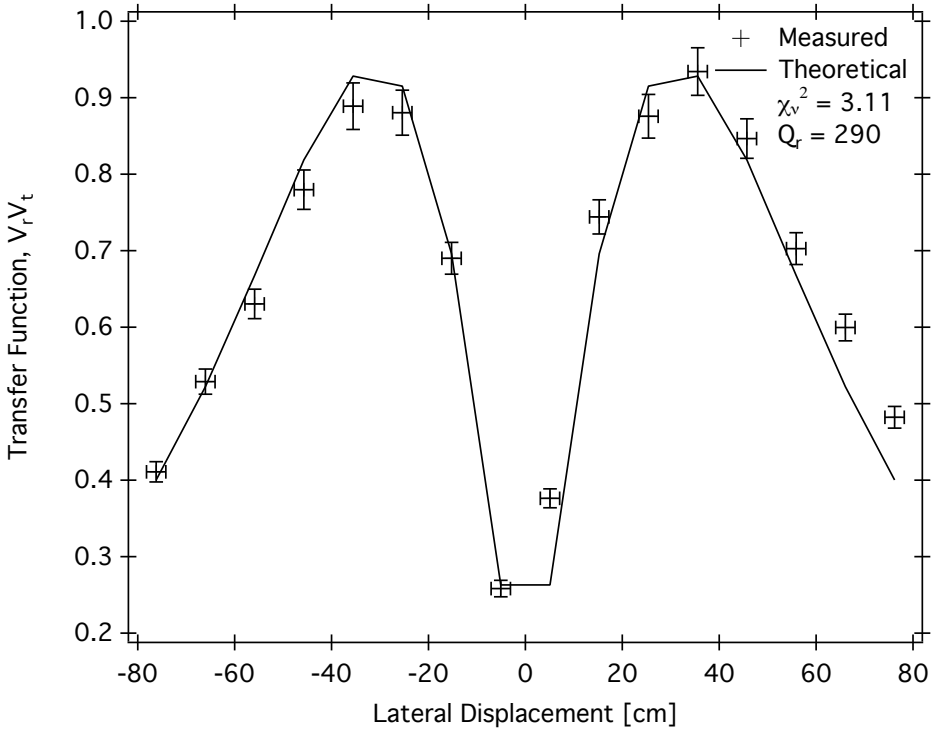

Figure 3.14: Comparison between measured and calculated transfer function of two oscillators with the receiving oscillator scanned laterally from -76 cm to 76 cm in 10 cm steps at a constant axial separation of 61 cm. The orientation of the receiver is at $\theta = 90°$. The point at 5 cm and at 76 cm were removed from the goodness of fit calculation yielding a final result of $\chi^2_\nu = 3.11$.

Chapter 4

Expanding To Three Oscillators

The previous chapter examined the two oscillator system in detail in order to gain confidence in the theoretical model. It also provided a means of testing and confirming the computation of mutual inductance for two circular loops used extensively in all comparisons. The ability to accurately predict the behaviour of this system was validated for almost all cases, with two notable exceptions. The first is a problem with the current experimental setup, in which it is difficult to maintain a constant relative angle between the receiving oscillator and the transmitting oscillator. The resulting orientational and positional errors lead to small errors in the experimental data. The second appears to be a limition of the model where the system begins to decrease the Q-factor at a certain magnitude of the coupling coefficient. The decrease is non-linear and can have a dramatic effect on the resulting measurments.

Armed with this knowledge, this chapter extends the model to include a third oscillator. There are two distinct experiments that result from adding an extra oscillator: one where the new oscillator is used as a transmitter and one where the new oscillator is used as a receiver. This logically splits the chapter into two sections. One will focus on the single transmitter - two receiver experiment and the second will focus on the two transmitter - single receiver case. The model will be tested to confirm whether it can accurately predict the transfer function between the oscillators while keeping in mind the lessons learned from the previous chapter, specifically the Q-spoiling. The chapter begins by extending the model in a gereral sense to three oscillators, then move to the specifics for the extra oscillator in its

respective section.

In the previous chapter, the receiving oscillator was oriented at different angles for various scans. This was to emphasize that the receiving oscillator orientation was accounted for in the model. This was verified and will not be further explored in this chapter. To simplify the system, the relative angular orientation of all receivers will be 0° for all of the experiments discussed. This will help make the results and comparisons more straightforward and succinct.

4.1 Extending the model

For three oscillators the system of equations is extended with another equation to account for the added oscillator. Again, using eqs. (2.6) and (2.12) the system of equations can be written out

$$\begin{pmatrix} \dot{a_1}(t) \\ \dot{a_2}(t) \\ \dot{a_3}(t) \end{pmatrix} = \begin{bmatrix} j\omega_1 - \Gamma_1 & j\omega_{12} & j\omega_{13} \\ j\omega_{21} & j\omega_2 - \Gamma_2 & j\omega_{23} \\ j\omega_{31} & j\omega_{32} & j\omega_3 - \Gamma_3 \end{bmatrix} \begin{pmatrix} a_1(t) \\ a_2(t) \\ a_3(t) \end{pmatrix} + \begin{pmatrix} F_1(t) \\ F_2(t) \\ F_3(t) \end{pmatrix}. \tag{4.1}$$

Transforming eq. (4.1) in the same manner as eq. (3.1) yields the following general form for three oscillators,

$$\begin{bmatrix} j(\omega - \omega_1) + \Gamma_1 & -j\omega_{12} & -j\omega_{13} \\ -j\omega_{21} & j(\omega - \omega_2) + \Gamma_2 & -j\omega_{23} \\ -j\omega_{31} & -j\omega_{32} & j(\omega - \omega_3) + \Gamma_3 \end{bmatrix} \begin{pmatrix} A_1 \\ A_2 \\ A_3 \end{pmatrix} = \begin{pmatrix} F_1 \\ F_2 \\ F_3 \end{pmatrix}. \tag{4.2}$$

All future analysis for three oscillators will originate from eq. (4.2). It should be emphasized that even though there is the possibility of having an external driving force, $F(t)$, on each oscillator, a real system will have some combination of RF-driven transmitting oscillators and undriven receiving oscillators. The receiving oscillators

will have their driving force term set to zero in order to satisfy that condition.

4.2 Two Receiving Oscillators

4.2.1 Theory

This section focuses on a single transmitting oscillator and two receiving oscillators. The starting point of the two receiving oscillators case is eq. (4.2). Important assumptions are all three oscillators are tuned to the same resonant frequency ($\omega_1 = \omega_2 = \omega_3 = \omega_0$) and the driving frequency is set to that same frequency ($\omega = \omega_0$). Therefore, the driving force terms for oscillators 2 and 3 are set to zero (*i.e.*: $F_2 = F_3 = 0$). This simplifies eq. (4.2) to

$$\begin{bmatrix} \Gamma_1 & -j\omega_{12} & -j\omega_{13} \\ -j\omega_{12} & \Gamma_2 & -j\omega_{23} \\ -j\omega_{13} & -j\omega_{23} & \Gamma_3 \end{bmatrix} \begin{pmatrix} A_1 \\ A_2 \\ A_3 \end{pmatrix} = \begin{pmatrix} F_1 \\ 0 \\ 0 \end{pmatrix} \tag{4.3}$$

Solving the system of equations using Cramer's rule gives the following relations for the amplitudes of the three oscillators:

$$A_1 = \frac{\Gamma_2\Gamma_3 + \omega_{23}^2}{detM} F_1 \tag{4.4}$$

$$A_2 = \frac{\omega_{13}\omega_{23} + j\omega_{12}\Gamma_3}{detM} F_1 \tag{4.5}$$

$$A_3 = \frac{\omega_{12}\omega_{23} + j\omega_{13}\Gamma_2}{detM} F_1 \tag{4.6}$$

and

$$detM = \Gamma_1\Gamma_2\Gamma_3 + \Gamma_1\omega_{23}^2 + \Gamma_2\omega_{13}^2 + \Gamma_3\omega_{12}^2 + j2\omega_{12}\omega_{13}\omega_{23} \tag{4.7}$$

Note that the amplitude is no longer 90° out of phase with the transmitter. The

phase is now a function of the coupling between all three oscillators. Therefore the overall phase of the system depends on the strength of the coupling between the other oscillators as well. The imaginary part shows the direct coupling between the transmitter and receiver as it did in the two-oscillator case, and the real part is the amplitude that is first transmitted from the transmitter to the other receiver and then re-transmitted to the receiver of interest. The term is real because every time the energy is transmitted from a transmitting oscillator to a receiving oscillator there is a phase shift of 90°.

Taking the ratio of the amplitudes of each receiver and the transmitter and taking the ratio of the receivers against each other are found using eqs. (4.4), (4.5) and (4.6) and give the following equations:

$$\frac{A_2}{A_1} = \frac{\omega_{13}\omega_{23} + j\omega_{12}\Gamma_3}{\Gamma_2\Gamma_3 + \omega_{23}^2} \tag{4.8}$$

$$\frac{A_3}{A_1} = \frac{\omega_{12}\omega_{23} + j\omega_{13}\Gamma_2}{\Gamma_2\Gamma_3 + \omega_{23}^2} \tag{4.9}$$

$$\frac{A_3}{A_2} = \frac{\omega_{12}\omega_{23} + j\omega_{13}\Gamma_2}{\omega_{13}\omega_{23} + j\omega_{12}\Gamma_3} \tag{4.10}$$

Due to the indistinguishability of the two receivers the ratios A_2/A_1 and A_3/A_1 have a similar form. Changing the expression from coupling coefficients and decay rates to measurable quantities (*i.e.*: self-inductance and mutual-inductance) and using the relation from eq. (2.19), eqs. (4.8), (4.9), and (4.10) become:

$$\frac{V_2}{V_1} = Q_2\frac{L_2}{L_1}\left(\frac{Q_3M_{13}M_{23} + jL_3M_{12}}{4L_2L_3 + Q_2Q_3M_{23}^2}\right) \tag{4.11}$$

$$\frac{V_3}{V_1} = Q_3\frac{L_3}{L_1}\left(\frac{Q_2M_{12}M_{23} + jL_2M_{13}}{4L_2L_3 + Q_2Q_3M_{23}^2}\right) \tag{4.12}$$

$$\frac{V_3}{V_2} = \frac{Q_3}{Q_2}\frac{L_3}{L_2}\left(\frac{Q_2M_{12}M_{23} + j2L_2M_{13}}{Q_3M_{13}M_{23} + jL_3M_{12}}\right) \tag{4.13}$$

These equations are now in a form that can be used for comparisons with experimental data. As with the system with two oscillators, the comparisons that are done in the next section are against the magnitude of eqs. (4.11), (4.12), and (4.13).

4.2.2 Results - Second Receiving Oscillator Axially Aligned

Two geometries were used to test the results for the system with two receivers. The first case has the first receiver is axially aligned with the transmitter then the second receiver is laterally scanned and the second case has the first receiver offset from the axis of the transmitter with the second receiver is laterally scanned. For simplicity, all scans have the relative angles for all of the oscillators set to 0°.

Beginning with the axially aligned receiver, the geometry of this experiment is found in Fig. 4.1. Using insight from the two oscillator case, the first receiver is just within range of the transmitter for Q-spoiling to have a small, but non-negligible effect on the amplitude on the first receiver. It is important to note that this may cascade the effects of Q-spoiling to the other receiving oscillator as the interaction between the two oscillators becomes non-negligible. The second receiver's axial separation is very short, implying that there will be very strong coupling and very strong Q-spoiling. The edges of the scan are outside of the critical coupling range and the results should match quite well with the model minus the effect of Q-spoiling on the first receiver.

Figs. 4.2, 4.3, and 4.4 show the results of comparing the theoretical and experimental curves. All the data is from the same scan where the first receiver is stationary and axially aligned with the transmitter at a distance of 61 cm. The second receiver is scanned latterally from -76 cm to 76 cm in 10 cm steps, identical to all the lateral scans in the two oscillator comparisons in the previous chapter.

Each plot compares the theoretical and experimental transfer functions. There are three transfer functions: the close receiver against the transmitter, the laterally

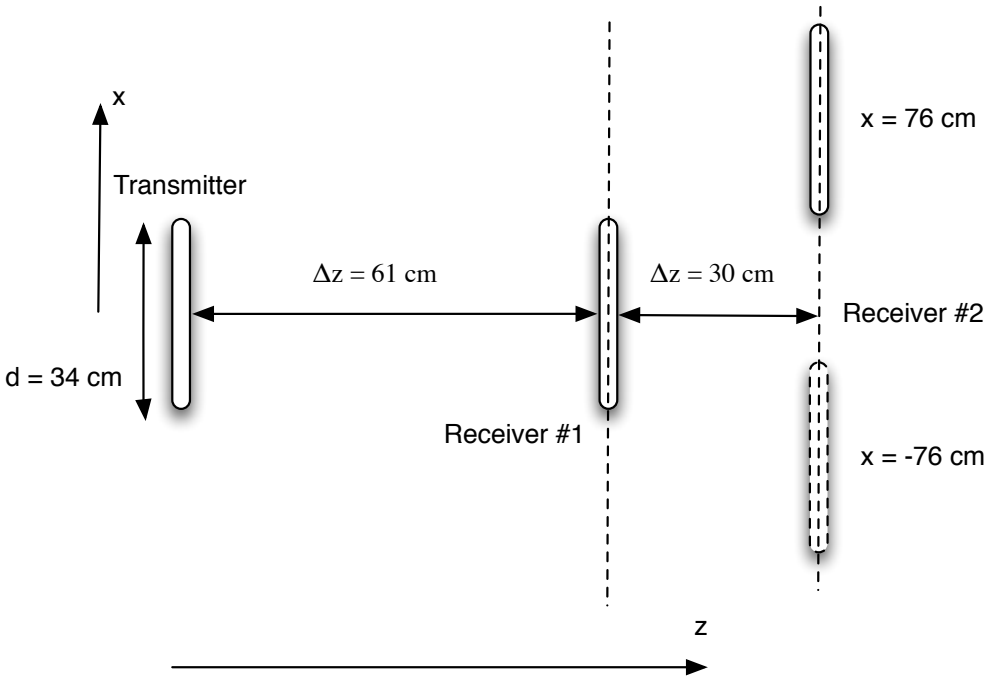

Figure 4.1: Schematic of the system with a single transmitter and two receivers. The first receiver is axially separated from the transmitter by 61 cm. The second receiver is axially separated from the first receiver by 30 cm. The second receiver is scanned laterally from -76 cm to 76 cm in 10 cm steps; identical to all of the lateral scans from the previous chapter.

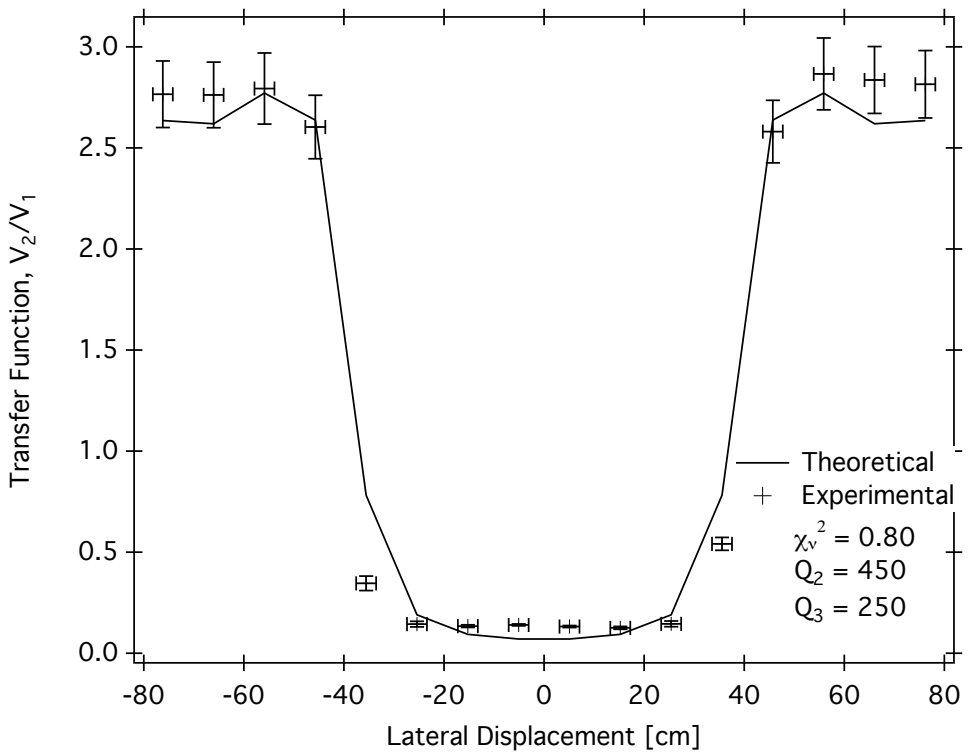

Figure 4.2: Theoretical and experimental comparison of the transfer function between the static receiver and the transmitter as the third receiver is laterally scanned. The dip in the middle is the effect of the other receiver on the system as the coupling becomes non-negligible. The Q-factor of the laterally scanned oscillator is 250, matching the fits from the previous chapter, and the new receiver has a Q-factor of 450. The goodness of fit for this plot is $\chi^2_\nu = 0.80$.

scanned receiver against the transmitter, and the laterally scanned receiver against the other receiver. All three are important to analyze due to the effects the other oscillators have in the system.

Fig. 4.2 compares the transfer function between the static receiving oscillator against the transmitting oscillator. The expected result for the transfer function between the two oscillators should remain constant until the coupling between the laterally scanned oscillator becomes substantial since neither oscillator is moving. As expected, as the second receiver nears the first receiver the second receiver begins to share in some of the energy stored in the system between the transmitter and first

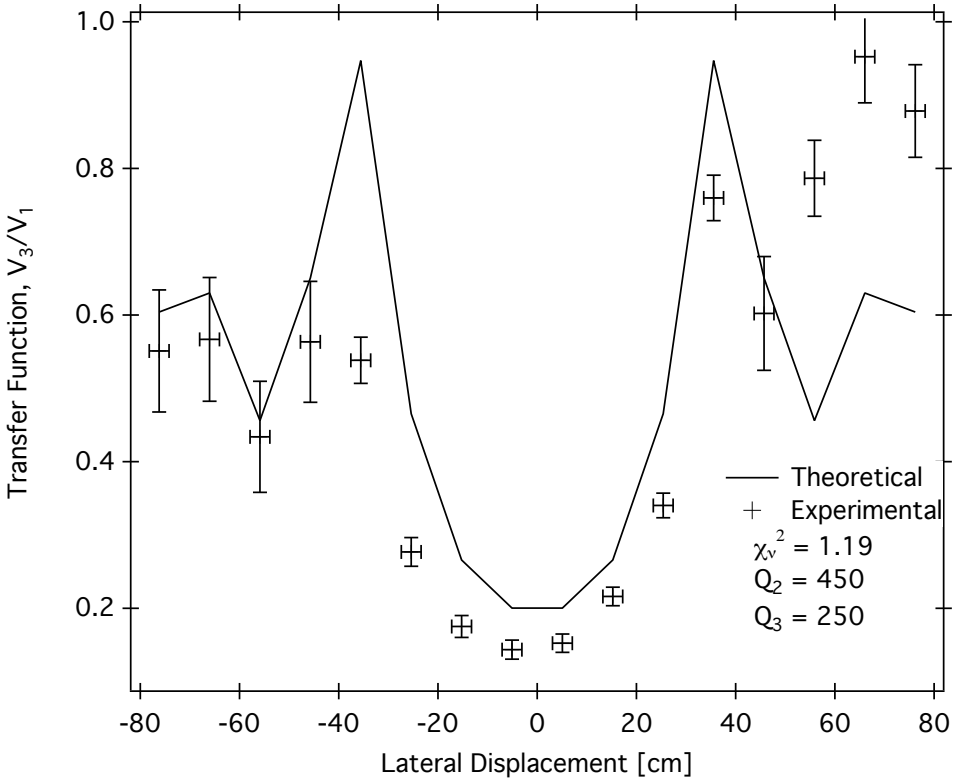

Figure 4.3: Theoretical and experimental comparison of the transfer function between the second receiver and the transmitter as the second receiver is laterally scanned. The Q-factor of the laterally scanned oscillator is 250, matching the fits from the previous chapter, and the new receiver has a Q-factor of 450. The outlier points have a lot of variation and large errors because the measurements were reaching the limits of the oscillator. Between -40 cm and 40 cm the shape qualitatively agrees, but the measured amplitude is lower than the predicted amplitude due to Q-spoiling. The χ^2_ν between the two curves is 1.19.

receiver. The curves agree well with a χ^2_ν of 0.80.

Fig. 4.3 compares the scanned receiving oscillator and the transmitting oscillator. There is a significant drop in the transfer function as the receivers near each other due to the strong coupling of the intermediate receiver. The measured values being all lower than the theoretical curve from -40 cm to 40 cm suggests Q-spoiling. The Q-spoiling could result from the static receving oscillator or due to the strong coupling between the two receiving oscillators in this region. Although the goodness of fit

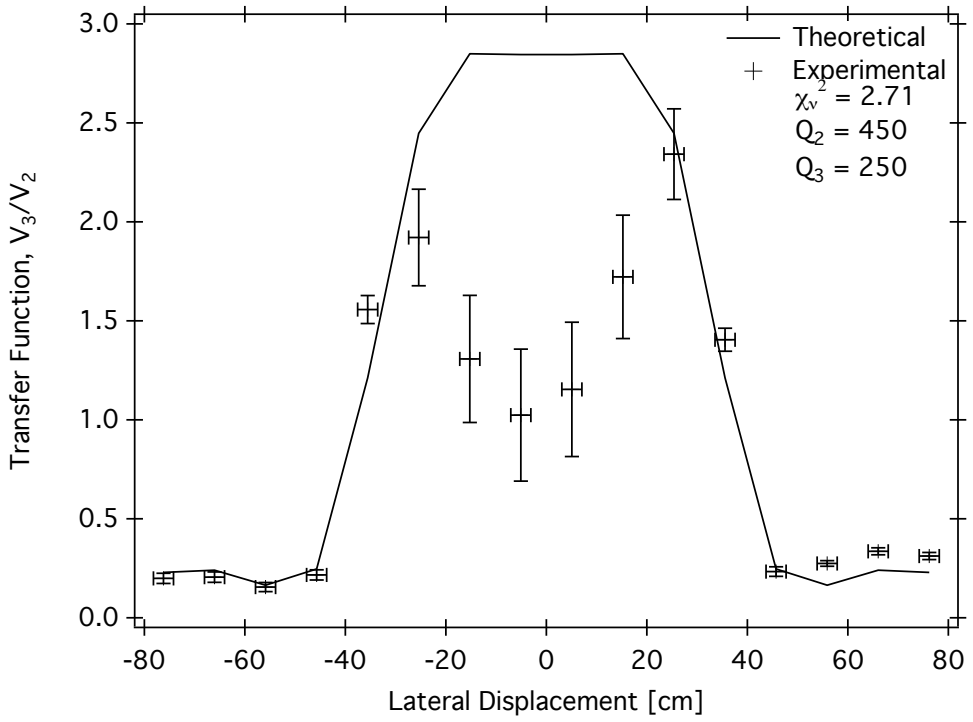

Figure 4.4: Theoretical and experimental comparison of the transfer function between the second receiver and the static receiver as the second receiver is scanned laterally. The Q-factor of the laterally scanned oscillator is 250, matching the fits from the previous chapter, and the new receiver has a Q-factor of 450. This plot is qualitatively similar to the two oscillator cases studied in the previous chapter. There is very strong Q-spoiling when the two receivers are very near to each other. Even without removing the points affected by Q-spoiling the curves agree fairly well with a χ^2_ν of 2.71.

is good with a χ^2_ν of 1.19, the plot is very noisy and it is difficult to make any quantitative statements with certainty. The errors are large near the edges of the plot due to measured values on the receiving oscillator being near the detection limit of the oscilloscopes.

Fig. 4.4 compares the scanned receiving oscillator to the static receiving oscillator. It shows a striking similarity to Fig. 3.10 with the expected Q-spoiling dip in the center of the plot. It agrees well except where the coupling is strongest between the two receiving oscillators and the Q-spoiling has the largest effect. An important aspect is that the static receiving oscillator appears to be screening the transmitting

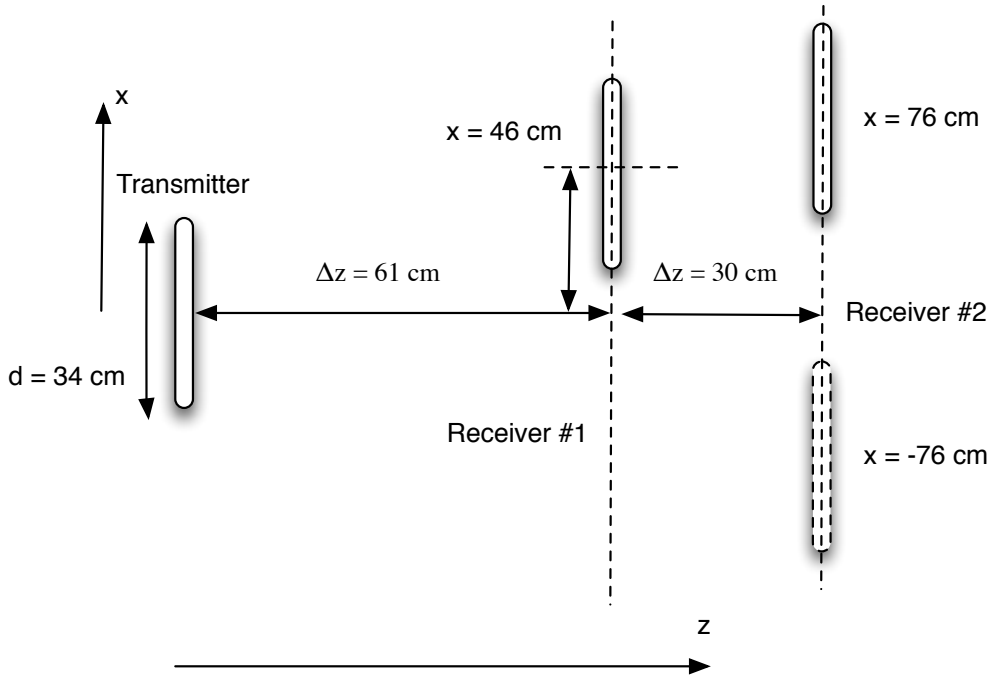

Figure 4.5: Schematic of the system with a single transmitter and two receivers. The first receiver is axially separated from the transmitter by 61 cm. The second receiver is axially separated from the first receiver by 30 cm, but is also laterally displaced by 46 cm. The second receiver is then scanned laterally from -76 cm to 76 cm in 10 cm steps.

oscillator. The static receiving oscillator appears as the only transmitter in the system from the perspective of other receiving oscillator. Most importantly, the curves match each other very well in the other regions not affected by strong Q-spoiling.

4.2.3 Results - Second Receiving Oscillator Axially Offset

The next experiment positions the static receiver offset from the axis defined by the transmitting oscillator. The rest of the scan conditions are identical to the previous system with two receiving oscillators. As with the previous system, all the oscillators have relative angles of 0° with respect to each other for simplicity. Fig. 4.5 shows a schematic of the system with the axially offset static receiving oscillator.

Fig. 4.6 compares the transfer function of the static receiving oscillator against

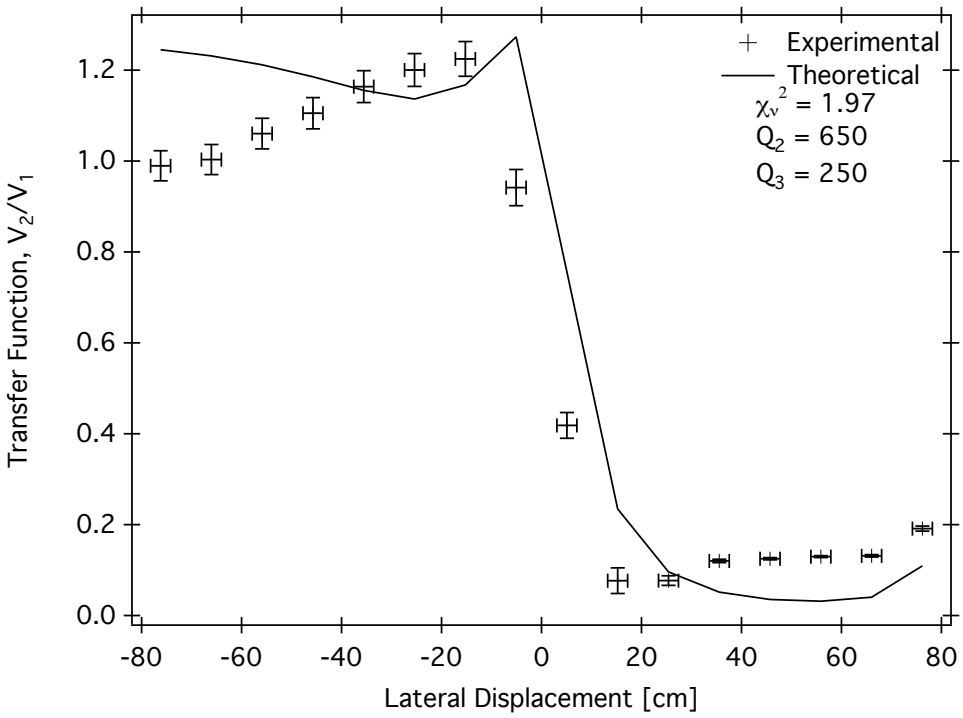

Figure 4.6: Theoretical and experimental comparison of the transfer function between the static receiver and the transmitter as the third receiver is scanned laterally. The Q-factor of the laterally scanned oscillator is 250, matching the fits from the previous chapter, and the new receiver has a Q-factor of 650. The drop in magnitude from 0 cm onwards is due to the effect of the coupling of the other receiver becoming significant. Even though the χ^2_ν of 1.97 is good, there appears to be some discrepancies between the expected curve and the measured values.

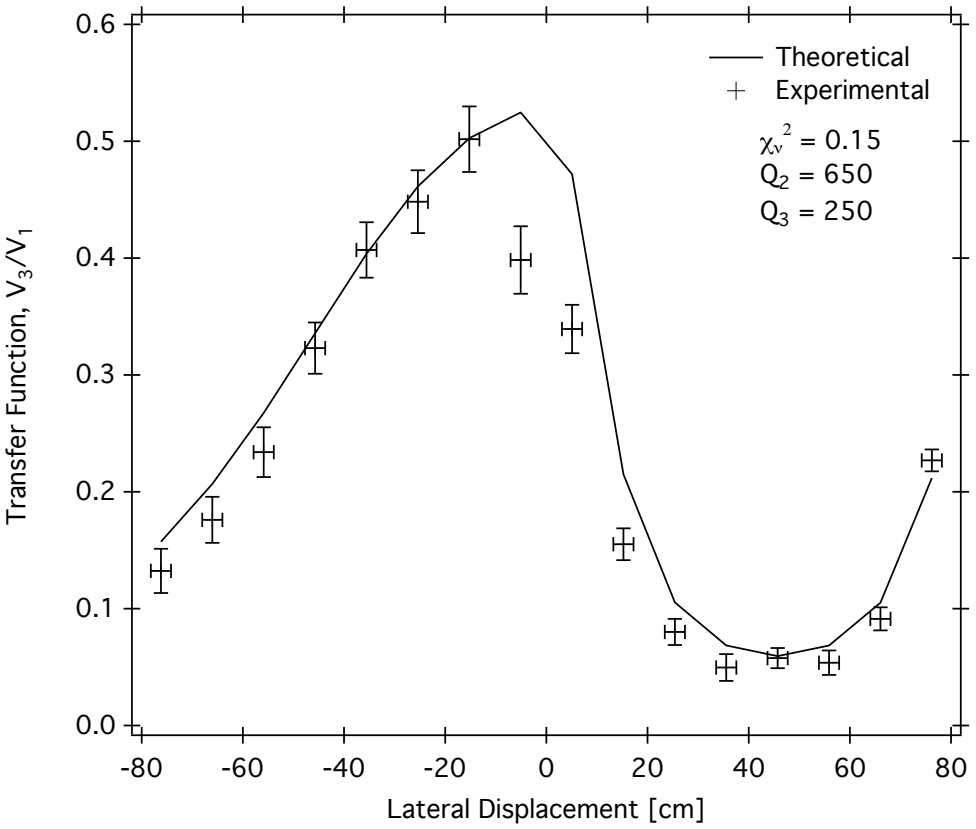

Figure 4.7: Theoretical and experimental comparison of the transfer function between the laterally scanned receiver and the transmitter as the second receiver is laterally scanned. The Q-factor of the laterally scanned oscillator is 250, matching the fits from the previous chapter, and the new receiver has a Q-factor of 650. The goodness of fit for the plot is very low with a χ^2_ν of 0.15. The dip beginning around 0 cm is due to the static receiver having extremely high coupling with the laterally scanned receiver.

the transmitting oscillator as the second receiving oscillator is scanned laterally from -76 cm to 76 cm in 10 cm steps. There is qualitative agreement between the two curves with the appropriate drop that begins at 0 cm matches the behaviour found in Fig. 4.2 as the coupling of the second receiving oscillator becomes significant. The Q-factor of the intermediate receiver is higher in this plot compared to the axially aligned intermediate receiver because there is no Q-spoiling from the transmitting oscillator to the static receiving oscillator.

Fig. 4.7 compares the transfer function of the laterally scanned receiving oscilla-

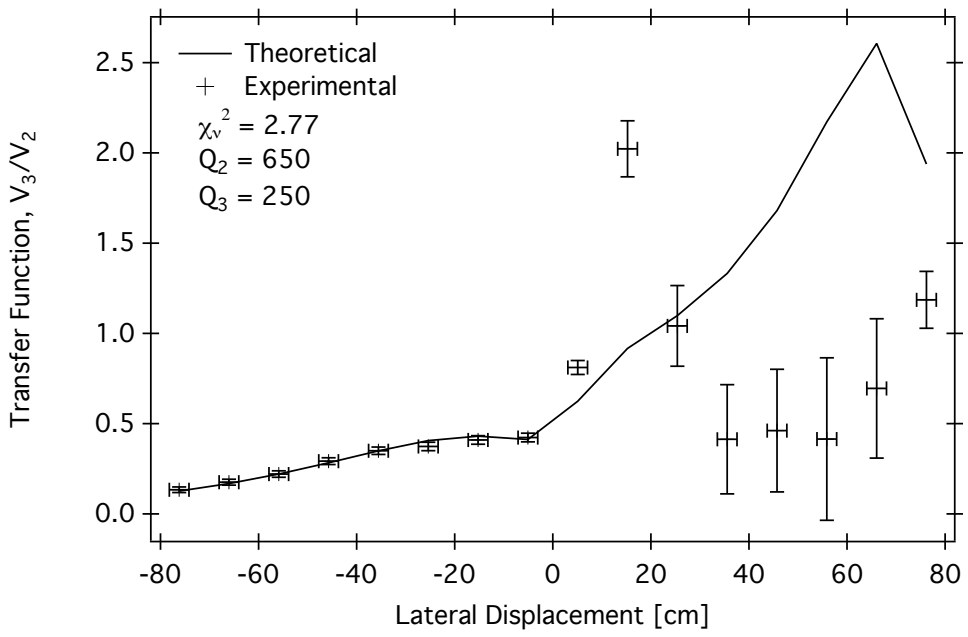

Figure 4.8: Theoretical and experimental comparison of the transfer function between the laterally scanned receiver and the static receiver as the second receiver is scanned laterally. The Q-factor of the laterally scanned oscillator is 250, matching the fits from the previous chapter, and the new receiver has a Q-factor of 650. There is very strong Q-spoiling when the two receivers are very near to each other.

tor and the transmitting oscillator. As with the plot found in Fig. 4.3, there is a dip in the curve as the coupling between the two receiving oscillators become significant. The stronger the coupling the lower the transfer function becomes. The curves agree extremely well with a very low χ^2_ν of 0.15.

Fig. 4.8 compares the transfer function of the laterally scanned receiving oscillator and the static receiving oscillator. It has a good agreement except where the coupling is strongest and where Q-spoiling has the largest effect. It appears that the static receiving oscillator is screening the transmitting oscillator, as it did in the axially aligned system. When the coupling between the two receiving oscillators is below the critical value the curves agree very well. Without removing any points from the goodness of fit, the plot has a χ^2_ν of 2.77. The plots rapidly diverge from

one another as the two oscillators near each other. The experimental plots indicate a much larger increase in the transfer function before Q-spoiling has a very substantial effect on the system. This implies that the model appears to underestimate the transfer function between two receivers when the Q-factors become extremely high (> 1000).

4.2.4 Conclusion - Two Receiving Oscillators

The system with two receiving oscillators has further confirmed that the model works when the coupling is high but not beyond the critical value found in the previous chapter due to Q-spoiling effects. It brought forth another limitation of the model by appearing to underestimate the magnitude of the transfer function when the Q-factors are extremely high. This is not surprising since the model is an extension of a linear approximation. This implies that when the oscillators have very high Q-factors the model would need to include more terms. The model agreement when the Q-factor is not very large and the coupling between the oscillators does not exceed the critical coupling is encouraging.

4.3 Two Transmitting Oscillators

4.3.1 Theory

Starting with eq. (4.2) for two transmitting oscillators by adding a second driving term, F_2. The resonant frequencies are again set to be equal with one another ($\omega_1 = \omega_2 = \omega_3 = \omega_0$) and the frequency of the driving force is set to the same

frequency as the resonant frequency ($\omega = \omega_0$) yielding a set of equations,

$$\begin{bmatrix} \Gamma_1 & -j\omega_{12} & -j\omega_{13} \\ -j\omega_{12} & \Gamma_2 & -j\omega_{23} \\ -j\omega_{13} & -j\omega_{23} & \Gamma_3 \end{bmatrix} \begin{pmatrix} A_1 \\ A_2 \\ A_3 \end{pmatrix} = \begin{pmatrix} F_1 \\ F_2 \\ 0. \end{pmatrix} \tag{4.14}$$

Using Cramer's yields the following equations for the amplitudes of each oscillator,

$$A_1 = \frac{(\Gamma_2\Gamma_3 + \omega_{23}^2)F_1 + (-\omega_{13}\omega_{23} + j\omega_{12}\Gamma_3)F_2}{detM} \tag{4.15}$$

$$A_2 = \frac{(-\omega_{13}\omega_{23} + j\omega_{12}\Gamma_3)F_1 + (\Gamma_1\Gamma_3 + \omega_{13}^2)F_2}{detM} \tag{4.16}$$

$$A_3 = \frac{(-\omega_{12}\omega_{23} + j\omega_{13}\Gamma_2)F_1 + (-\omega_{12}\omega_{13} + j\omega_{23}\Gamma_1)F_2}{detM} \tag{4.17}$$

and

$$detM = \Gamma_1\Gamma_2\Gamma_3 + \Gamma_1\omega_{23}^2 + \Gamma_2\omega_{13}^2 + \Gamma_3\omega_{12}^2 + j2\omega_{12}\omega_{13}\omega_{23} \tag{4.18}$$

In this set of equations the receiving oscillator amplitude has a similar form as the receiving oscillators of the system with two receiving oscillators; the exception being a contribution from each transmitting oscillator. There are two contributions to the transmitting oscillator amplitudes. One is similar to the expected form seen in eqs. (3.8) and (4.4) and is attached to its corresponding drive term. The other contribution has a similar form as the receiving oscillators in the system with two receiving oscillators. These terms show that the energy is transmitted directly from the other transmitting oscillator and from indirect transmission through the receiving oscillator. Note that the transmitting oscillators are no longer purely real quantities.

Unfortunately, the system with two transmitting oscillators is not as straightforward as the systems previously discussed. Determining the transfer function for the previous systems, due to the simplicity of having a single driving force term, required dividing the receiving oscillator amplitude by the transmitting oscillator

amplitude. Unfortunately, the system with two transmitting oscillators, all three of the amplitudes are a function of both transmitter amplitudes, (ie: $A_n = f(F_1, F_2)$ where n represents any of the three amplitudes). This complicates determining a transfer function that has a convenient form. To combat this problem, the receiving oscillator amplitude can be transformed with a specific choice of variable transform. Instead the"driving forces", F_1 and F_2, will be mapped to be functions of the amplitudes, A_1 and A_2. Using a transform of this kind will allow the receiving oscillator amplitude to be a function of the transmitter *amplitudes* (ie: $A_3 = f(A_1, A_2)$. The benefit of this approach is that it easily leads to determining the AC voltage of the receiver as a function of the AC voltage of the transmitters.

Mapping the receiving oscillator amplitude from a function of the driving forces to the amplitudes was done in the following manner. Consider the two transmitting oscillator amplitudes, A_1 and A_2, as a column vector, $\boldsymbol{A}$, and the driving forces as another column vector. The coefficients in front the driving forces become a 2×2 matrix, M, and can be represented as,

$$\boldsymbol{A} = M\boldsymbol{F} \tag{4.19}$$

where M is equal to,

$$M = \frac{1}{detM}\begin{bmatrix} \Gamma_2\Gamma_3 + \omega_{23}^2 & -\omega_{13}\omega_{23} + j\omega_{12}\Gamma_3 \\ -\omega_{13}\omega_{23} + j\omega_{12}\Gamma_3 & \Gamma_1\Gamma_3 + \omega_{13}^2 \end{bmatrix}. \tag{4.20}$$

Inverting this system of equations maps the variables to the desired form,

$$\boldsymbol{F} = M^{-1}\boldsymbol{A} \tag{4.21}$$

with the inverted matrix given as,

$$M^{-1} = \frac{1}{\Gamma_3}\begin{bmatrix} \Gamma_1\Gamma_3 + \omega_{13}^2 & \omega_{13}\omega_{23} - j\omega_{12}\Gamma_3 \\ \omega_{13}\omega_{23} - j\omega_{12}\Gamma_3 & \Gamma_2\Gamma_3 + \omega_{23}^2 \end{bmatrix} \tag{4.22}$$

Substituting F_1 and F_2 directly into eq. (4.17) and simplifying the result yields the following relation for A_3,

$$A_3 = j\frac{\omega_{13}}{\Gamma_3}A_1 + j\frac{\omega_{23}}{\Gamma_3}A_2. \tag{4.23}$$

This is a remarkably simple result that shows that the amplitude of one of the receiver is the algebraic sum from each transmitter. Converting this result into one with measurable quantities using eq. (2.19) yields the following result for the AC voltage of the receiving oscillator.

$$V_3 = jQ_3\left(\frac{M_{13}}{L_1}V_1 + \frac{M_{23}}{L_2}V_2\right). \tag{4.24}$$

4.3.2 Results - Two Transmitting Oscillators

Testing the system with two transmitting oscillators will take a somewhat different approach than the system with two receiving oscillators. Rather than having two distinct cases to explore, only one geometry will be used but at many different distances. The geometry shown in Fig. 4.9 illustrates the series of scans were performed. The two transmitters were separated by 46 cm within the same plane. The receiving oscillator was scanned laterally across the two transmitting oscillators at different axially seperated distances of 30 cm, 61 cm, 91 cm, and 122 cm. The receiving oscillator was kept at a relative angle of 0° and the transmitters remained fixed for all scans. Based on the results from the previous experiments, the model and experiments agree when the oscillators are not within the region where Q-spoiling due to critical coupling becomes significant. The receiver is scanned at four distances

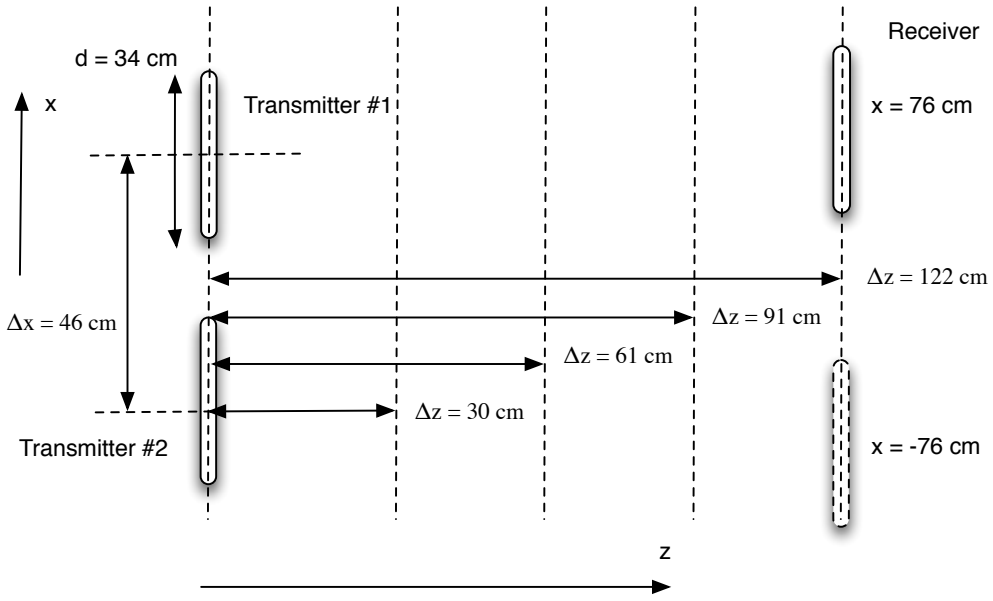

Figure 4.9: Schematic for the system with two transmitters and a single receiver. This experiment is a set of four lateral scans at different distances of axial separation. The transmitters were separated by a distance of 46 cm from centre to centre. The axial separations are 30 cm, 61 cm, 91 cm, and 122 cm. The receiver is laterally scanned from -76 cm to 76 cm in steps of 10 cm.

to gain further insight into this aspect of the system. The scan at 30 cm should be so close that the model does not agree. The scan at 61 cm should exhibit some Q-spoiling. The last two scans should agree with the model.

Fig. 4.10 compares the measured voltage on the receiving oscillator against the voltage expected by the model with the receiving oscillator at an axial separation of 30 cm. The receiving oscillator was scanned laterally from -76 cm to 76 cm in 10 cm steps. The fitted theoretical curve required a Q-factor of 175. This is much lower than expected due to extreme Q-spoiling. More important, the shape does not match either. The χ^2_ν for the comparison was 1876. The Q-spoiling is strong enough in this regime that every almost every experimental point was affected. This agrees with the results found in the system with two receiving oscillators where the model didn't agree when the two receiving oscillators were extremely close to each other. There appears to be more quenching near the -40 cm as shown since there is

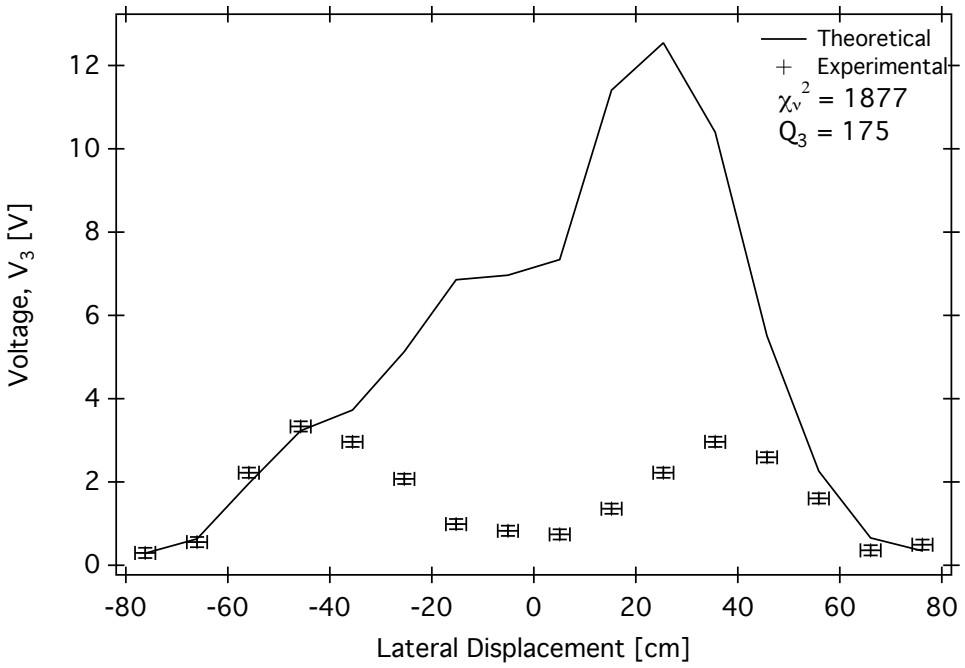

Figure 4.10: Comparison of the model and experiment of the voltage on the receiving oscillator at an axial separation of 30 cm. The receiving oscillator was scanned from -76 cm to 76 cm in 10 cm steps. The Q-factor on the receiver was found to be 350. The theoretical curve does not match the experimental curve with a χ^2_ν of 1876.

no second peak in the theoretical curve.

Fig. 4.11 compares the measured voltage on the receiving oscillator against the voltage expected by the model with the receiving oscillator at an axial separation of 61 cm. The receiving oscillator was scanned laterally from -76 cm to 76 cm in 10 cm steps. The fitted Q-factor remained 175, but the curve has a shape reminiscent of the Q-spoiling observed in previous plots. Ignoring the middle six points (points from -20 cm to 20 cm) in the goodness of fit produces a χ^2_ν of 2.39. The overall reduction in the Q-factor is likely due to the receiver always undergoing some Q-spoiling always being in the critical coupling area of both of the transmitting oscillators. The two transmitting oscillators are undergoing Q-spoiling from each other because their coupling is $\omega_{12}/\omega_0 = 0.0068$, further reducing the output for the entire system.

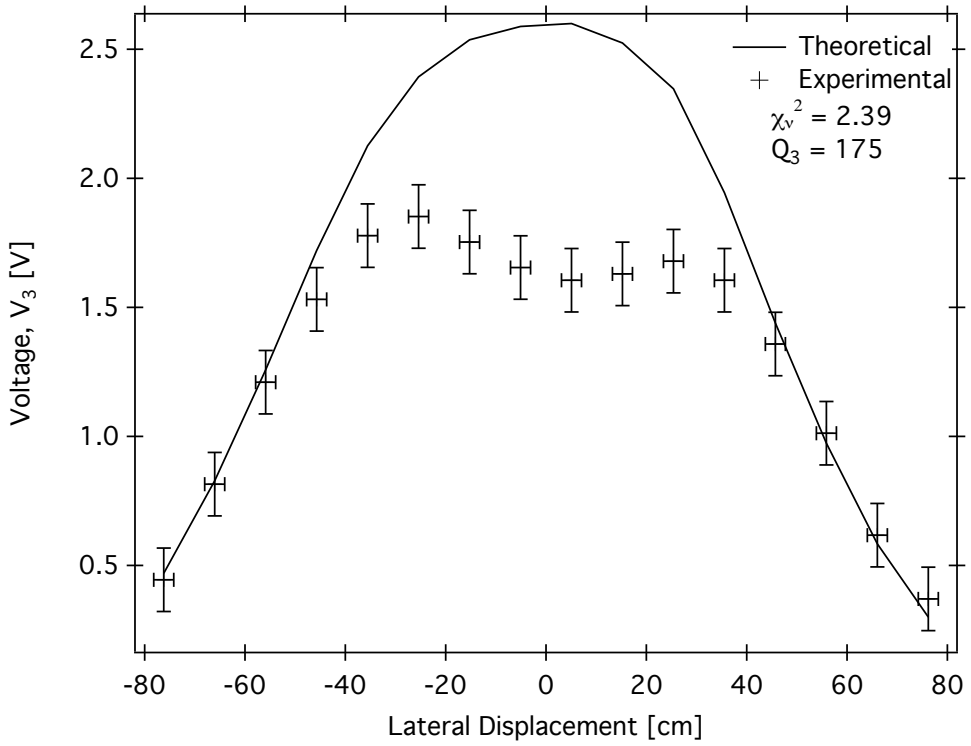

Figure 4.11: Comparison of the model and experiment of the voltage on the receiving oscillator at an axial separation of 61 cm. The receiving oscillator was scanned from -76 cm to 76 cm in 10 cm steps. The Q-factor on the receiving oscillator was found to be 175. The curves are similar to other comparisons where Q-spoiling affects the middle couple points in a dramatic way but otherwise matches well. The goodness of fit had a χ^2_ν of 2.39 when not including the middle six points from -20 cm to 20 cm.

Having the entire system always being under the effect of Q-spoiling necessarily reduces the overall Q-factor used to fit the data.

Fig. 4.12 compares measured voltage on the receiving oscillator against the voltage expected by the model with the receiving oscillator at an axial separation of 91 cm. The receiving oscillator was scanned latterally from -76 cm to 76 cm in 10 cm steps. The curves agree very well with each other with a χ^2_ν of 1.01 when using a Q-factor of 195. Knowing from the previous two cases that the two transmitting oscillators are Q-spoiled, the curve being a good fit while not having a Q-factor of 250 is plausible. This comparison provides strong evidence that the model works

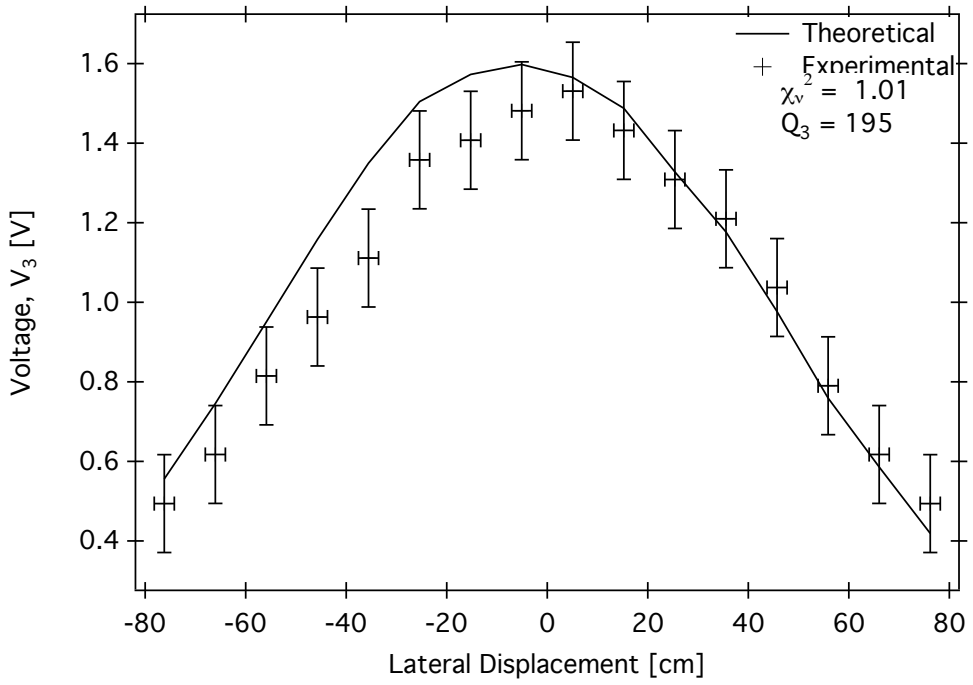

Figure 4.12: Comparison of the model and experiment of the voltage on the receiving oscillator at an axial separation of 91 cm. The receiving oscillator was scanned from -76 cm to 76 cm in 10 cm steps. The Q-factor on the receiver was found to be 390. The curves fit very well where the goodness of fit, χ^2_ν, was 1.01.

as expected if Q-spoiling is taken into account.

Fig. 4.13 compares measured voltage on the receiving oscillator against the voltage expected by the model with the receiving oscillator at an axial separation of 122 cm. The receiving oscillator was scanned latterally from -76 cm to 76 cm in 10 cm steps. The curves were fit with a Q-factor of 215 and agree well with a χ^2_ν of 0.11. The χ^2_ν is very low because all of the data points were taken near the detection limits of the oscilloscope and therefore the error bars are proportionally larger than in other scans. At this distance there is no Q-spoiling from either of the two transmitting oscillators to the receiving oscillator, but the Q-spoiling between the two transmitting oscillators still reduces the expected Q-factor. This provides further evidence that the coupling between the two transmitters decreases the overall

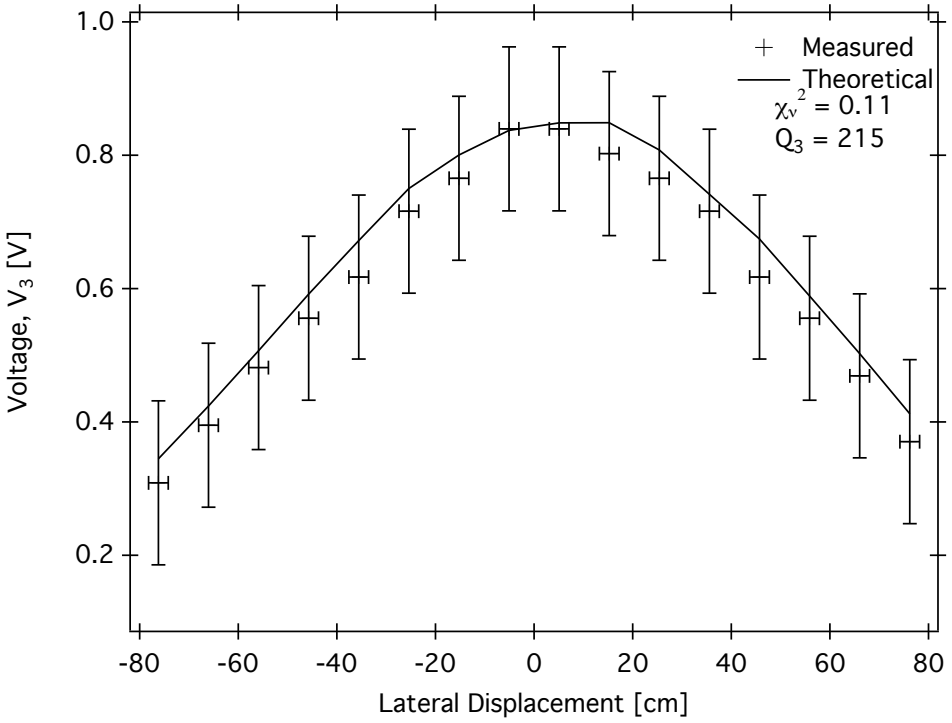

Figure 4.13: Comparison of the model and experiment of the voltage on the receiving oscillator at an axial separation of 122 cm. The receiving oscillator was scanned from -76 cm to 76 cm in 10 cm steps. The Q-factor on the receiver was found to be 430. The curves fit very well where the goodness of fit, χ^2_ν, was 0.11. The low χ^2_ν is due to the measurements being near the detection limits of the oscilloscope.

amount of energy available to be transferred to the receiving oscillator.

4.3.3 Conclusion - Two Transmitting Oscillators

The model was confirmed to be accurate for the system with two transmitting oscillators. Q-spoiling is still very apparent in this system and must be taken into account for Q-factors being smaller than expected. When the coupling was apparent, but not overwhelming, the plots had similar features seen in many of the other plots where Q-spoiling was apparant. Although the Q-factors are not explicitly part of the eq. (4.24), if the transmitting oscillators are spoiling each other, that will manifest in the overall energy transfer measured on the receiving oscillator.

Chapter 5

Engineering Aspects

5.1 Engineering Challenges

There are many problems that can arise when trying to use resonant coupling to achieve wireless energy transfer. The first is to ensure that the resonant frequency of every oscillator in the system is tuned to the same resonant frequency within ω_0/Q. If resonant frequency of any oscillator drifts too far from the driving frequency then the overall performance of the system quickly degrades.

Another challenge is the Q factors for all oscillators must be as high as possible ($Q > 100$). In order to achieve high Q values for all the oscillators, all loss mechanisms must be minimized. Components must be chosen with care to ensure that they are made of low loss materials, minimal stray capacitance, etc..

Finally, the experimental results strongly suggest a Q-spoiling effect due to non-linear losses in the invisible thin oxide layer on the copper antenna loops. This could be mitigated in future systems by the use of silver plated antennas. This is quite common in RF systems.

5.2 The Quality Factor

The Quality Factor "Q factor" or simply Q of an electronic oscillator is a dimensionless measure of the total damping rate of the oscillations due to various energy loss mechanisms. These energy loss mechanisms may be desirable (e.g. extraction of

useful power), parasitic (e.g. undesired radiation), or dissipative (e.g. conversion of electrical power to heat via resistance, dielectric losses, eddy current heating, etc.).

There are many examples of the Q factor for an oscillator that is either a series or parallel resonant RLC circuit. This work contains a system that is somewhat more complicated and will be discussed in the context of a parallel resonant LC circuit in parallel with a resistance R with a resistance r in series with the inductor, as shown in Fig. 5.1.

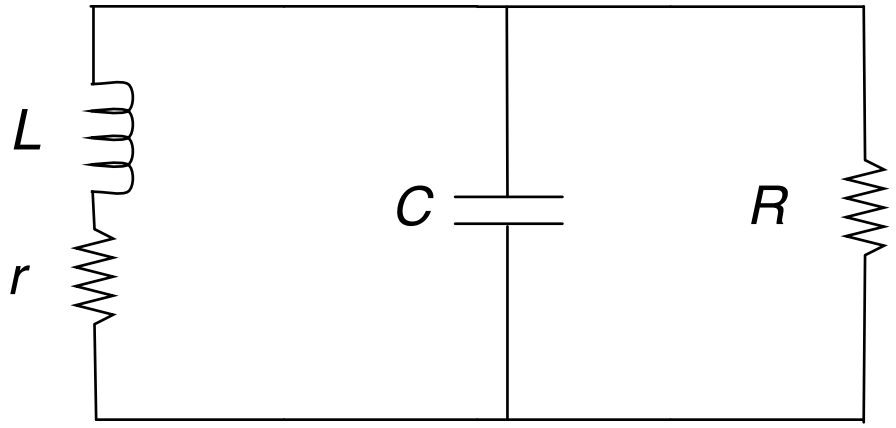

Figure 5.1: Schematic for the RLC resonant circuit as an example of this system. R is the total equivalent parallel resistance and r is the total equivalent series resistance.

If R is the only parallel loss in the system then Q is given by the formula $Q = R/\omega_0 L$ where $\omega_0 = 1/\sqrt{LC}$ is the resonant frequency of the oscillator without losses. If r is the only series loss in the system then Q is given by the formula $Q = \omega_0 L/r$.

In very high Q circuits R and r will not be a real physical external resistor; rather it will be an effective equivalent resistance which accounts for all the loss mechanisms which act to reduce the Q of the system. There are some important points to note about a system like this:

(a) It makes clear that having a large parallel R ($\omega_0 L \ll R$) and small series r ($r \ll \omega_0 L$) tends to increase Q. The smaller $\omega_0 L$ is relative to R, the less current

flows in R and the lower the dissipative rate. Conversely, for smaller r relative to $\omega_0 L$ minimizes the power dissipated in an element that must have current flow through it regardless. For the parallel losses, the limit of $R \to \infty$ yields $Q \to \infty$ and for series losses the limit of $r \to 0$ yields $Q \to \infty$.

(b) R is suggestive of parallel leakage currents in the capactior dielectric leading to dielectric loss. r is suggestive of internal parameters such as intrinsic resistances.

(c) Multiple parallel loss mechanisms are accommodated in this model by writing R as a parallel equivalent

$$\frac{1}{R} = \frac{1}{R_1} + \frac{1}{R_2} + ... + \frac{1}{R_n}. \tag{5.1}$$

Since $Q = R/\omega_0 L$, the above relation can be rewritten as

$$\frac{1}{Q} = \frac{\omega_0 L}{R} = \frac{\omega_0 L}{R_1} + \frac{\omega_0 L}{R_2} + ... + \frac{\omega_0 L}{R_n}, \tag{5.2}$$

reducing to

$$\frac{1}{Q} = \frac{1}{Q_1} + \frac{1}{Q_2} + ... + \frac{1}{Q_n} \tag{5.3}$$

where $Q_i = R_i/\omega_0 L$ is the value of Q which would be achieved if the loss mechanism leaking to the equivalent parallel resitance R_i were the only loss in the system.

(d) Multiple series loss mechanisms are accommodated in this model by writing r as a series equivalent

$$r = r_1 + r_2 + ... + r_n \tag{5.4}$$

and a similar argument can be made for the series losses with $Q = \omega_0 L/r$ where

$$\frac{1}{Q} = \frac{r}{\omega_0 L} = \frac{r_1}{\omega_0 L} + \frac{r_2}{\omega_0 L} + ... + \frac{r_n}{\omega_0 L}, \tag{5.5}$$

reducing to

$$\frac{1}{Q} = \frac{1}{Q_1} + \frac{1}{Q_2} + ... + \frac{1}{Q_n} \tag{5.6}$$

where $Q_i = \omega_0 L/r_i$ is the value of Q which would be achieved if the loss mechanism leaking to the equivalent parallel resitance r_i were the only loss in the system.

All the series and parallel components Q-factors can be combined together such that the overall system Q-factor,

$$\frac{1}{Q} \approx \frac{1}{Q_s} + \frac{1}{Q_p}. \tag{5.7}$$

This allows all of the individual quality factors to be added together easily. Since it is possible to identify several physically distinct loss mechanisms in a real circuit, this is a helpful approach. Two additional useful observations are:

(a) Q will always be lower than the lowest individual Q_i.

(b) In the limit where one individual Q_i is significantly lower than the rest, $Q \approx Q_i$.

These observations make it clear that the path to higher Q is achieved by attacking the weakest links in the chain (i.e. dealing with the lower Q_i) first. The Q will increase gradually as smaller loss mechanisms are eliminated by circuit improvements, etc..

5.3 Limits on the Quality Factor

For resonant wireless power transfer applications a high quality factor Q is required. A list of the different loss mechanisms and their associated effect on Q is: the resistance of the coil(Q_{res}), radiation loss due to the radiation resistance (Q_{rad}), the internal losses due to the dielectrics in external capacitors (Q_{die}), eddy currents

induced in metal objects in the environment (Q_{eddy}), and losses to the external environment (Q_{ext}). The 10 MHz regime, the primary limitation is the resistance of the coil itself followed by the radiation resistance of the antenna. We combine these loss mechnanisms as described above:

$$\frac{1}{Q} = \frac{1}{Q_{res}} + \frac{1}{Q_{rad}} + \frac{1}{Q_{die}} + \frac{1}{Q_{eddy}} + \frac{1}{Q_{ext}} \tag{5.8}$$

Therefore, knowing how the different mechanisms scale is quite important; potentially saving time when attempting to build a system with a Q higher than the theoretical maximum or to give insight into why the measured Q is substantially different than what was calculated. The following discussion considers each loss mechanism separately in turn.

The resistive loss is due to the finite resistance of the coil. The oscillators were built of copper, which has a small but non zero resistivity $\rho \simeq 1.7x10^{-8}\ \Omega m$. Although more expensive, silver is a marginally better conductor with $\rho \simeq 1.6x10^{-8}\,\Omega m$. The losses due to the current flowing in the copper coil may be modelled by a small series resistance r as follows.

For the high frequency ($\omega/(2\pi) \sim 10\ MHz$) and high conductivities ($\rho \sim 10^{-8}\Omega m$) used in our systems, the skin effect becomes important. Conduction currents flow in a layer pealing at the conductor surface and decaying exponentially with characteristic length δ, known as the skin depth. Using the well known formula for the skin depth,

$$\delta = \sqrt{\frac{2\rho}{\omega\mu_0}} \tag{5.9}$$

(numerically copper has a skin depth of 20.8 μm at 10 MHz) a wire of length s and radius a has

$$r_{int} = \frac{\rho s}{2\pi a\delta} = \frac{s}{2\pi a}\sqrt{\frac{\rho\omega\mu_0}{2}}. \tag{5.10}$$

This enables the quality factor Q to be expressed as follows:

$$Q_{res} = \frac{\omega L}{r_{int}} = L\frac{2\pi a}{s}\sqrt{\frac{2\omega}{\mu_0 \rho}} \tag{5.11}$$

For a fixed geometry the quality factor can be improved by increasing the frequency of operation, but only as $\sqrt{\omega}$. However, one cannot increase the frequency ω arbitrarily because of other losses which increase with frequency. There are also physical limitations on how much the frequency can be increased. For a given coil winding, the only way to increase the resonant frequency is to reduce the parallel capacitance. This cannnot be reduced arbitrarily due to physical limitations of physical capacitors.

Resistive losses in the coil can be eliminated using superconductive coils. While superconductive coils are used in precision measurement systems and can allow very high Q's to be achieved ($Q > 10000$ [10]), they require cryogenic cooling and making practical large scale applications unlikely.

The next significant loss mechanism is power loss due to radiation of electromagnetic waves. For loop-type coils radiation will be dominantly magnetic dipole radiation. For a loop-type antenna composed of N identical loops the effective "radiation resistance" is givn by

$$r_{rad} = \frac{8}{3}\eta\pi^3\left(\frac{NA_{loop}}{\lambda^2}\right), \tag{5.12}$$

where η is the characteristic impedance of the medium and $\lambda = 2\pi c/\omega$ is the radiation wavelength in vacuum. The corresponding Q factor is

$$Q_{rad} = \frac{\omega_0 L}{r_{rad}} = \left(\frac{6\pi c^4}{\eta}\right)\left(\frac{L}{N^2 A_{loop}}\right)\frac{1}{\omega^3}. \tag{5.13}$$

It shows that Q_{rad} dependends strongly on frequency. As the frequency increases the

quality factor decreases dramatically and loop antennas are effective radiators at high MHz frequencies. Although not lost in the same manner as the internal resistance, the power lost due to radiation is inaccessible since it is transmitted into the far-field of the antenna. This reduces the energy available to the resonant near-field antenna system that is performing the wireless energy transfer. Fig. 5.2 illustrates how Q_{int} and Q_{rad} affect the overall quality factor of a sample coil system as frequency is increased.

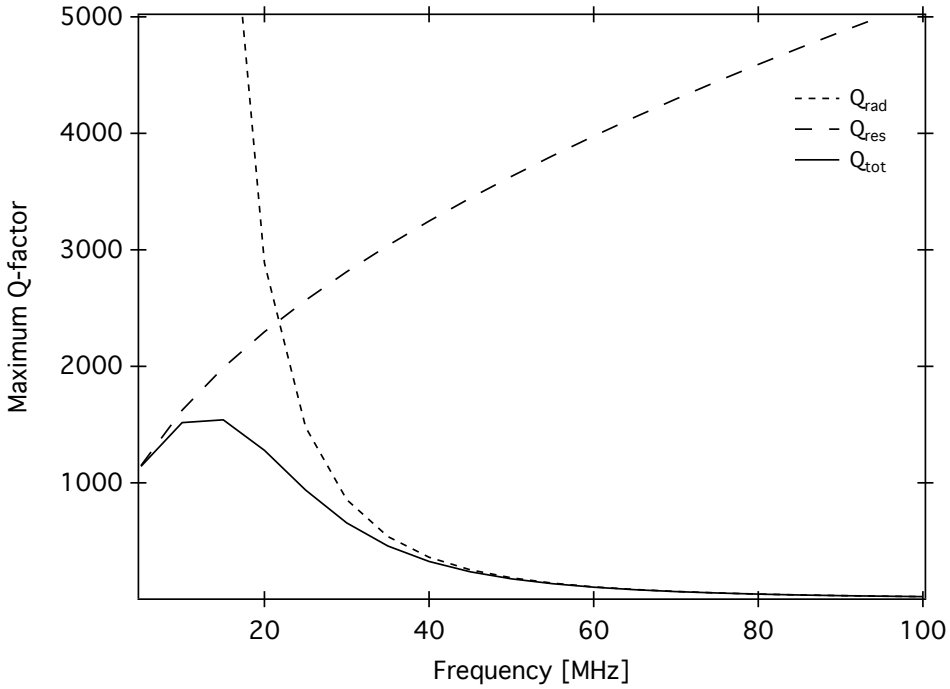

Figure 5.2: Plot comparing Q_{res} and Q_{rad} as the frequency of the system is increased. The overall Q-factor Q_{tot} illustrates that the Q-factor of the overall system is always lower than any individual Q-factor.

The next term represents the dielectric losses in the discrete capacitors. Capacitor dielectric materials vary widely depending on the capacitance value, physical size of the capacitor, working voltage, operating temperature, etc. Each dielectric material has a complex permittivity $\epsilon = \epsilon_R + j\epsilon_I$ where the real part of the permittivity is

responsible for setting the value of the capacitance via

$$C = \frac{\epsilon_R A_{eff}}{d_{eff}}, \tag{5.14}$$

and the imaginary part of the permittivity (ϵ_I) determines the losses, which may be modelled as an effective resistance in parallel

$$R_{eff} = \frac{\epsilon_R}{\epsilon_I} \frac{1}{\omega C}. \tag{5.15}$$

In useful dielectrics, the imaginary component is much smaller than the real component ($\epsilon_I \ll \epsilon_R$). This would yield the following limit on the quality factor,

$$Q_{disc} = \frac{R_{eff}}{\omega_0 L} = \frac{\epsilon_R}{\epsilon_I} = \frac{1}{\tan\delta}, \tag{5.16}$$

where $\tan\delta = \epsilon_I/\epsilon_R$ is known as the "loss tangent" of the dielectric and is tabulated for many materials. Note that $\tan\delta$ is the standard notation and δ is unrelated to the skin depth δ_{skin}. The loss tangent depends strongly on frequency, but is highly material dependent [11]. Ceramic chip capacitors are available in the RF 1-100 MHz domain. They typically have loss tangents of $\epsilon_I/\epsilon_R \simeq 0.0001$, and as such would limit the Q to ∼10 000, well above the limits imposed by resistive and radiation losses.

The next term represents the losses due to lossy dielectric properties if the resonant circuit was fabricated on a printed circuit board (PCB). As such, Q_{die} can be considered to be the upper limit of Q imposed by the loss tangent of the PCB board material. The permittivity of the PCB material and the geometry of the spiral coil will determine the magnitude of the distributed stray capacitance C_{stray} which in parallel with the externally added discrete chip capacitance $C_{discrete}$ will determine the total lumped capacitance $C = C_{stray} + C_{discrete}$, which determines the resonant

frequency of the circuit $\omega_0 = 1/\sqrt{LC}$.

For an inductance coil of fixed geometry fabricated on a given PCB material the inductance L and stray capacitance drive the requirements for $C_{discrete}$. The inevitable imperfection in manufacturing tolerances for a given coil printing processes will result in variations in coil dimensions and hence inductance L_m from coil to coil, and thus slightly different values of $C_{discrete}$ will be required from board to board. Alternatively, a technique such as laser trimming might be used post-printing to trim each coil inductance to the same value within the needed tolerance, in much the same manner as is done for metal-film resistors. It is important to note that the requirement for tuning frequencies to resonance becomes more stringent as the tank circuit Q increases. Values of the loss tangent for dielectric PCB materials are well tabulated across different frequencies and vary from relatively high values (i.e. lossy boards) for conventional PCB materials (loss tangent $\sim$0.04 for FR4 or GTEK) to much lower losses for specialty ceramic board materials such as Rogers RO4003 (loss tangent $\sim$0.003). Remember the stray capacitance C_{stray} appears in parallel with $C_{discrete}$, the total value of Q due to all dielectric losses Q_{cap} is given by

$$\frac{1}{Q_{cap}} = \frac{1}{Q_{disc}} + \frac{1}{Q_{die}} = \frac{\omega_0 L}{R_{eff,disc}} + \frac{\omega_0 L}{R_{eff,die}} = \left(\frac{C_{disc}}{C}\right)\tan\delta_{disc} + \left(\frac{C_{stray}}{C}\right)\tan\delta_{stray}, \tag{5.17}$$

where $C = C_{disc} + C_{die}$ is the total capacitance of the tank circuit oscillator and $\tan\delta_{disc} = (\epsilon_I/\epsilon_R)_{disc}$ and $\tan\delta_{die} = (\epsilon_I/\epsilon_R)_{die}$ are the loss tangents of the discrete and stray capacitances, respectively. This shows the relative contribution of each capacitive component is in proportion to its contribution to the total capacitance, and thus the requirement on the loss tangent of the PCB material used is less stringent as long as the contribution of the stray capacitance is kept small. This is another reason for not pushing the operating frequency too high. As the frequency is increased for a fixed total inductance the total capacitance must decrease, making the ratio C_{stray}/C

increase its contribution to the maximum Q-factor. This would make the choice of PCB material much more important if this was the case.

The next term represents the loss contributed by eddy currents induced in nearby metal objects. Such objects act ase non-resonant pickup coils, and the eddy currents induced in them will be damped by the metal resistivity, which can be fairly high for iron-based alloys. This damping manifests itself as an additional loss mechanism, but is highly dependent on the configuration of external objects. If the state of location is not known exactly, it would be impossible to estimate this value *a priori*. However, it is important to be aware of the effect and its potentially significant adverse effect on the resonant circuit Q when operating in proximity to ferromagnetic structures.

The final term represents all additional loss mechanisms not accounted for in the above discussion. There are a myriad of such effects: poor solder joints, lossy oxide layers (a serious problem for copper), lossy grease residue. In practice, measured values of Q achieved experimentally are never as high as those predicted based on the above loss accounting procedure. Since the final value of Q is always limited by the most lossy mechanism, the stringency dealing with extra losses requires more care as the targeted value of Q increases. Thus for room temperature copper coils in the MHz region, values of $Q \sim 20$ can almost always be achieved, values of $Q \sim 100$ require more care in coil design and construction, values of $Q \sim 1000$ are definitely achievable, but require considerable care and attention to detail, while values of $Q \sim$ 10 000 are probably not routinely achievable unless the system is brought into a cryogenics regime. Note that superconducting resonant circuits can achieve values of $Q \sim 50\ 000$, limited by the loss tangent of the dielectrics used [10].

In practice, because values of Q can only be predicted with modest accuracy, it is necessary to experimentally measure them, and use the measured values of Q when comparing resonant wireless power transfer model predictions with experimental results. For example, for the 30 cm diameter single-turn circular loop coils made

of 0.25 inch = 6.35 mm diameter copper refrigerator tubing used for most of out experiments, the two leading order loss mechanisms were resistive losses and radiative losses. At the frequency of interest of ∼10 MHz yields the corresponding values $Q_{int} = 1600$ and Q_{rad} =23 000 for a total tank circuit $Q = (Q_{int}Q_{rad})/(Q_{int}+Q_{rad}) =$ 1500, but in practice the coils achieved were closer to 1000 on average. Kurs *et al.* working at 9 MHz with helical copper coils and no external discrete capacitor achieved similar values [1].

5.4 Potential challenges

The inductor for the LC system is an antenna must be very clean. Having electrical tape glue stuck onto the antenna can lower the Q since the glue can act as an additional lossy oxide layer. Finally, there is the problem of isolating the system from the environment. This is a catch-22 since the entire point of building the system in the first place is to transfer energy to other objects in the environment. This leads to the problem where the rest of the outside world becomes another loss mechanism that must be accounted for. Unfortunately, there is no way compensate for these mechanisms beforehand. The types of objects that can potentially cause problems are other large metal objects that act like non-resonant pick up coils. In essence, it is adding an arbitrary number of loads that must then compete with the receiver of interest.

There is another challenge associated with the isolating the system. Calibrating the system is difficult because the probe must have an extremely high parallel impedance and add minimal stray capacitance while it is in contact with the system. Depending on the location, this might imply that the system is calibrated on site to ensure any stray effects are accounted. Ideally, the more isolated the system the easier it to predict the performance.

The final concern is connecting the power system to the device of interest. Care is required for ensuring the resonant loops are not quenched by the load it is meant to drive. This likely means that contactless non-resonant transmission will be required to get the useful energy out of the resonant system. The load may add stray capacitance that might require small adjustments to ensure the resonant frequency is the matched for all elements of the system. None of these elements may come into play, but it is important to recognise that a great many things could dramatically affect this system.

5.5 Safety concerns with time varying fields

Since resonant wireless energy transfer involves large-amplitude RF **E** and **B** fields, extra attention is required to not exceed the exposure limits expressed by the International Committee for Non-Ionizing Radiation Protection (ICNIRP) and the Institute for Electrical and Electronic Engineers (IEEE). The document published by the ICNIRP is an in-depth study [12] of the effects of time varying fields and how the effects change at different frequencies. At the end of the document they summarize the highest recommended field exposures for **E** and **B** by frequency range. All the experiments using resonant wireless energy transfer have been performed in the 1-10 MHz regime and should be discussed explicitly. There are two distinguishing levels for time varying fields. If someone works in areas with fields present for an 8 hour work day, their recommended exposure limits are higher than the general public exposure limits. The equations for **E** and **B** for occupational exposure are:

$$\boldsymbol{E} = \frac{610}{f(\text{MHz})}\ [\text{V/m}] \tag{5.18}$$

$$\boldsymbol{B} = \frac{2.0}{f(\text{MHz})}\ [\mu\text{T}] \tag{5.19}$$

The experiments in this thesis have been carried out at 10 MHz and therefore the recommended exposure limits are: E = 61 V/m and B = 200 nT. For the general public, the equations are the following for acceptable exposure:

$$\boldsymbol{E} = \frac{87}{\sqrt{f(\text{MHz})}}\ [\text{V/m}] \tag{5.20}$$

$$\boldsymbol{B} = \frac{0.92}{f(\text{MHz})}\ [\mu\text{T}] \tag{5.21}$$

which gives acceptable exposure limits of: E = 27.5 V/m and B = 92 nT.

Calculating the theoretical values for the near-field (see Appendix A):

$$\mathbf{B} = \frac{\mu m}{4\pi R^3}\left(\hat{\mathbf{R}} 2\cos\theta + \hat{\boldsymbol{\theta}}\sin\theta\right) \tag{5.22}$$

$$\mathbf{E} = -\hat{\boldsymbol{\phi}}\frac{j\omega\mu m}{4\pi R^2}\sin\theta \tag{5.23}$$

.

These fields exhibit angular dependence (see geometry in Appendix A). The system in this thesis will be used as an example at an $\theta = 0°$. At $\theta = 0°$, only the magnetic field has a non-zero value. The geometry is described in appendix C. The system is in air making μ become μ_0. A test distance for medium range, $R = 50$ cm will be used. This leaves the only unknown as the current, providing an upper limit for the current in the loop. At this geometry the maximum current is 813 mA. Based on this example, unless the systems are in isolated areas, the applications of this technology are limited to low power systems.

Although potentially discouraging, there still are many applications where using wireless energy transfer would be useful. For example, nuclear reactors or chemical plant components where workers would not be near major pieces of equipment on a regular basis. This technology would likely be most useful for smaller electronic power supply where significant electric power transfer is required in a hazardous en-

vironment, running wires or power cables is not an option or as a means to power floating high voltage systems. Unfortunately, these limitations don't allow for wireless energy transfer systems to be mounted everywhere, dramatically reducing some commercial market share for powering consumer devices except for some very low power applications.

Chapter 6

Concluding Remarks

6.1 Summary

In this thesis, a mathematical framework was presented to model the behaviour of a strongly resonant system used for medium range wireless power transfer. Based from the original work by Kurs [1], the model was fleshed out to yield equations that could be used by engineers to design systems for delivering useful amounts of power; primarily the voltage on the individual oscillators and the transfer function for determining the amount of energy can be usefully transferred. Starting from the basis equations using the complex amplitudes discussed in Haus [6] and showing how the amplitudes are solved for an arbitrary number of oscillators was discussed in Chapter 2.

The equations in terms of complex amplitudes and coupling coefficients and not in a form familiar to most RF and power engineers. To be of better use, the relations needed to be in terms of voltage and current. The optoelectronic forms of the equations were transformed into currents and voltages. The model was compared to the experiment by setting up a system where two or three oscillators were simultaneously coupled to each other. To focus effort, all of the equations were expressed in terms of voltages. This is due to voltages being easier to measure in a non-destructive way since coupling with external sources dramatically reduces the Q-factor of the oscillators. The voltages can be directly used to find the transfer function between any two oscillators.

In order to probe the system without excessive perturbations, a very large resistance was placed in parallel (greater than 1 MΩ). Within the resistance there was a 10:1 voltage divider to measure the voltage for each oscillator. In order to not couple any of the oscillators, separate oscilloscopes were used for each oscillator; otherwise, the oscillators will couple to each other through the probes and quench their high Q-factors. The Q-factors for all three oscillators used in the experiment were 500 or greater. Having high Q-factors made the system is easily succeptible to other influences - including oscilloscopes and other large metal objects. Therefore, extra care must be taken to ensure that external effects cannot spoil the quality of the system.

The model was developed to for systems involving two and three oscillators. For two oscillators, it is straightforward to assign one as a transmitter and the other a receiver. For three oscillators there are two distinct cases: a single transmitter with two receivers and two transmitters with a single receiver. Experimental data was collected for all three systems and compared. The specific geometry used in the experiments used circular loops of equal size for all three oscillators. Using circular loops permitted the use of an analytical solution for determining the mutual inductance. The solution was valid for any geometry of the oscillators - allowing for direct comparisons and minimizing the use of approximations.

The experimental data showed many agreements with the theoretical predictions. The two oscillator case showed excellent agreement with the model for various orientations of the receiver with respect to the transmitter. However, there appears to be a significant spoiling of the Q-factor at a critical value of the coupling coefficient between the oscillators. This spoiling manifests itself in the systems with three oscillators as well. The critical value for this system was $\omega_{ij}/\omega_0 = 0.00212$. The spoiling is strong enough to dramatically alter the shape of the curves. The trademark of the Q-spoiling in this work is the double peaked in the response instead of

the expected single bell shaped curve. The Q-spoiling appears to be directly related to the coupling strength between any two oscillators because the only parameter that varies with position is the mutual inductance. Since the mutual inductance was verified independently and compared in the same regions where the Q-spoiling was prominent and agreed extremely well, the Q-spoiling is attributed to the nonlinear losses in the invisible oxide layer on the copper antennas at a critical electric field.

Some of the challenges with a system of this type were also discussed. Engineering challenges about external elements that quench the strong coupling of the system can ruin the entire system. The system needs to be electrically isolated from all possible external loads that are not the load of interest. It is difficult to achieve in absolute terms but there are ways to mitigate these effects. Various system loss contributions that set the upper limits on the quality factor were also discussed. Using this knowledge the system can be built specifically to minize the effect of the different loss mechanisms. Unfortunately, it is not easily calculated beforehand because many effects are highly non-linear and appear only in certain situations.

The quality factor was used as fitting parameters specifically for this reason. The real quality factor will always being lower than the ideal quality factor because the load will necessarily reduce the quality factor. This analysis was useful when building the system and can be used to recognize that the system is behaving worse than anticipated. It isolates specific mechanisms that can be limiting the system and provide a systematic way to tackle each mechanism on its own to achieve the highest possible quality factor.

Finally, the effects of exposure to RF-electric and magnetic fields on the human body were discussed. This is important for all applications of this work because it introduces another design criterion. There are limits to the maximum field strength the general population can be exposed to and therefore the scope of distributing power in this manner requires careful planning.

6.2 Future Work

There are two primary areas where future work would be of benefit continued research in this area. First is looking thoroughly into the mechanism of the Q-spoiling effect. Second is to remake the system based on all of the lessons learned from the prototype used in this work.

Based on the experiments done, there appears to be a specific coupling value where the Q-spoiling becomes dominant. The spoiling also appears to be non-linear. It would be extremely important to discover what are the dominant factors that affect the critical value of coupling, if any. Does the shape and size of the oscillators have an effect? Is the relative geometry important? Are there systems where the effect does not appear? These are questions that should be answered with future work. This would require building many systems of varying oscillator shapes and system geometries to fully map out that parameter space. Have a precise understanding of the Q-spoiling would be of great design tool for modeling the behaviour *a priori*.

There are two core changes that a new system would derive benefit. First and foremost, the oscillators should not be made of copper. Copper oxide forms easily on the surface and for the purposes of this system has a very large loss tangent. The ideal material should be a good conductor and either have a slow grow rate of the lossy oxide or the oxide not have as high of a loss tangent. Using a silver or having a silver coating thicker than the skin depth should help mediate this loss mechanism and extend the reliability of the system.

Second, making the system more compact would allow more precise measurements to be easier to perform. The large oscillators were very cumbersome and ensuring the exact location and orientation of each loop was difficult. Motorizing the system in an effort to take as much data as possible would ensure more accurate comparions. It would be important to ensure that the motors themselves do not

interfere with the system itself. Any material that must come into contact with the oscillators should be made of teflon or a similar material for structural stability and minimizing the external effects on the system. Finally, in cases where the voltages that are measured are of the same magnitude as many of the measurements performed here, then low noise pre-amps would be required to amplify the signal and minimize the uncertainty in the measurements.

References

[1] A. Kurs *et al.* Wireless power transfer via strongly coupled magnetic resonances. *Science*, 317(5834):83–86, 2007.

[2] N. Tesla. Apparatus for transmitting electrical energy. *U.S. Patent 1 119 732*, 1914.

[3] University of Saskatchewan Space Design Team. Space elevator. *www.usst.ca*, 2009.

[4] B. Cannon *et al.* Magnetic Resonant Coupling As a Potential Means for Wireless Power Transfer to Multiple Small Receivers. *IEEE Transactions on Power Electronics*, 24(7):1819–1825, JUL 2009.

[5] S. Valtchev *et al.* Resonant contactless energy transfer with improved efficiency. *IEEE Transactions on Power Electronics*, 24(3), March 2009.

[6] H. Haus. *Waves and Fields in Optoelectronics*. Prentice Hall, 1984.

[7] F. Bloch *et al.* Magnetic resonance for nonrotating fields. *Physical Review*, 57(6):522–527, MAR 1940.

[8] L. Allen *et al.* *Optical Resonance and Two-Level Atoms*. Dover Publishing, 1975.

[9] L. Solymar. *Lectures on Electromagnetic Theory*. Oxford University Press, 1984.

[10] R. Weisskoff. rf squid detector for single-ion trapping experiments. *J. Appl. Phys.*, 63:4599–4604, May 1988.

[11] D. Pozar. Microwave engineering. 1998.

[12] ICNIRP. Guidelines for limiting exposure to time-varying electric, magnetic, and electromagnetic fields (up to 300 ghz). *Health Physics*, 74:494–522, 1998.

[13] N. Ida. *Engineering electromagnetics; 2nd ed.* Springer, New York, NY, 2004.

[14] II Rabi. Space quantization in a gyrating magnetic field. *Physical Review*, 51(8):0652–0654, APR 1937.

[15] D. Griffiths. *Introduction to Quantum Mechanics*. Prentice Hall, 2nd edition edition, 2005.

[16] G. Harnwell. *Principles of Electricity and Magnetism*. McGraw Hill, 2nd edition edition, 1949.

[17] H. Wheeler. *Pire*, 16(1398), 1928.

[18] C. Snow. *Formulas for Computing Capacitance and Inductance*. U.S. Govt. Print. Off., 1954.

[19] J. Maxwell. *A Treatise on Electricity and Magnetism*. Dover Publications INC, New York, 1954 (reprint from original from 1873).

[20] S. Babic *et al.* Validity check of mutual inductance formulas for circular filaments with lateral and angular misalignments. *Progess In Electromagnetics Research*, Vol. 8:15–26, 2009.

[21] F. Grover. The calculation of the mutual inductance of circular filaments in any desired positions. *Proceedings of the I.R.E.*, pages 620–629, Oct. 1944.

[22] C. Akyel *et al.* Mutual inductance calculation for non-coaxial circular air coils with parallel axes. *Progess In Electromagnetics Research*, PIER 91:287–301, 2009.

[23] F. Grover. *Inductance Calculations*. Dover, New York, 1964.

[24] K. Kim *et al.* Mutual inductance of noncoaxial circular coils with constant current density. *IEEE Trans. Mag.*, Vol. 33(No. 5):3916–3921, Sep. 1997.

[25] J. Conway. Inductance calculations for circular coils of rectangular cross section and parallel axes using bessel and struve functions. *IEEE Transactions on Magnetics*, Vol. 46(No. 1), January 2010.

Appendix A

Antenna Theory

In the theory of antennas [13], there are two fundamental antennas from which the majority of practical antennas can be derived: the electric dipole antenna and the magnetic dipole (or "loop") antenna. Most common antennas found in devices such as cellphones and radios are based on one or the other of these two basic antennas. The analysis in this project focuses on loop antennas, therefore only the magnetic dipole antenna will be discussed.

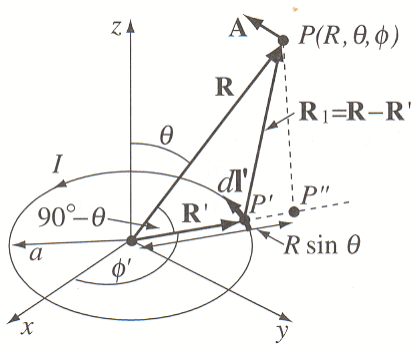

Figure A.1: Geometry for Magnetic Dipole Antenna [13]. I is the current in the loop, a is the radius, $d\mathbf{l}'$ is the elemental line segment of the loop, **R** is the distance from the origin to point P, **R'** is the distance to the point P' on the loop.

Consider a small loop, as described in Fig. A.1, carrying a current varying sinusoidally in time. A small loop implies that the radius is much smaller than the wavelength, λ, of the field ($a \ll \lambda$). The time-retarded magnetic vector potential, **A**, is [13]:

$$\mathbf{A} = \hat{\boldsymbol{\phi}} \frac{\mu m}{4\pi R^2} (1 + j\beta R)\, e^{-j\beta R} \sin\theta \left[\frac{Wb}{m}\right] \tag{A.1}$$

From this, the magnetic field intensity, **H**, and electric field, **E**, can be obtained:

$$\begin{aligned}\mathbf{H} &= \frac{\mathbf{B}}{\mu} = \frac{\boldsymbol{\nabla} \times \mathbf{A}}{\mu} \\ &= -\hat{\mathbf{R}}\frac{j\omega\mu\beta^2 m}{2\pi\eta}e^{-j\beta R}\cos\theta\left(\frac{1}{(j\beta R)^2}+\frac{1}{(j\beta R)^3}\right) \\ &\quad -\hat{\boldsymbol{\theta}}\frac{j\omega\mu\beta^2 m}{4\pi\eta}e^{-j\beta R}\sin\theta\left(\frac{1}{j\beta R}+\frac{1}{(j\beta R)^2}+\frac{1}{(j\beta R)^3}\right) \end{aligned} \tag{A.2}$$

$$\begin{aligned}\mathbf{E} &= \frac{\boldsymbol{\nabla} \times \mathbf{H}}{\epsilon} \\ &= \hat{\boldsymbol{\phi}}\frac{j\omega\mu\beta^2 m}{4\pi}e^{-j\beta R}\sin\theta\left(\frac{1}{j\beta R}+\frac{1}{(j\beta R)^2}\right) \end{aligned} \tag{A.3}$$

Where μ is the magnetic permeability of the medium in which waves propagate, ϵ is the electric permittivity of the medium in which waves propagate, $m = IA_{loop}$ is the magnetic dipole moment of the loop and A_{loop} is the area of the loop, $\beta = 2\pi/\lambda$ is the "wave number" (rads/m), $\omega = 2\pi f$ is the angular frequency (rads/s) with f being the frequency, and $\eta \equiv \sqrt{\mu/\epsilon}$ is the impedance of the medium in which waves propagate.

The purpose of an antenna is to launch electromagnetic waves. The radiated electromagnetic power per unit area (Watt/m^2) is given by the Poynting vector,

$$\mathbf{P} = \mathbf{E} \times \mathbf{H} \tag{A.4}$$

For the total radiated power to be constant, the Poynting vector must therefore fall off as $1/R^2$ which implies that $E \propto 1/R$ and $H \propto 1/R$. This region is what is known as the wave zone or the far-field. In this regime, as $R \to \infty$ only the $1/R$ terms of the electric and magnetic field are significant; these terms allow for propagating wave solutions and is what allows many wireless communications technologies that are available to operate.

For the wireless energy transfer of current interest, the receiver needs to be near the antenna. When near to the antenna the higher order terms in $1/R$ dominate and the electric and magnetic fields become,

$$\mathbf{H} = \frac{m}{4\pi R^3}\left(\hat{\mathbf{R}}2\cos\theta + \hat{\boldsymbol{\theta}}\sin\theta\right) \tag{A.5}$$

$$\mathbf{E} = -\hat{\boldsymbol{\phi}}\frac{j\omega\mu m}{4\pi R^2}\sin\theta \tag{A.6}$$

Since the electric field is only proportional to $1/R^2$, its contribution to the overall field is negligible compared to the magnetic field. This region is called the near-field because the fields in this region are not proportional to $1/R$ and therefore there are no electromagnetic waves. In fact, the field looks identical to an oscillating magnetic dipole and in this region the magnetic energy is being stored, much like an inductor.

Taking a closer look at the magnetic field, it is obvious why previous attempts

at wireless energy transfer were not pursued since the magnitude of the field decays extremely rapidly ($\propto 1/R^3$.) It is for this reason that transformer windings are extremely close together (in fact they are interlaced in order to maximize the magnetic flux coupling from one side to the other.) Driving the coils at a tuned resonant frequency is going to overcome this barrier. This was first noticed and developed by the MIT researchers [1] based on resonant coupling techniques well known in the optical domain.

Appendix B

Coupled Oscillators RWA and the Undriven Solution

The following appendix describes how the current analysis is analogous to the Rotating Wave Approximation in atomic systems. The first section describes the two-level atomic system and the following sections are the undriven case using coupled-mode theory to illustrate how the two solutions are analogous.

B.1 Rotating Wave Approximation Method

Consider a two level atomic system with an external applied field that varies sinusoidally. To analyze the system, time-dependent perturbation theory can be used and a solution for the probability of being in a particular state can be found. If the applied field is near the resonant frequency of the system then the solution for how the probability of being in a particular state evolves sinusoidally (as seen in Fig. B.1.) Unfortunately, this treatment breaks down as the probability of being in the higher state approaches unity. Since the solution is in the form of a wave, it has both a forward component and a backwards component to the wave. If the backwards component is initially neglected then an exact solution for the probability can be found. This was first done by Rabi [14] and is known formally as the rotating wave approximation. It was for this reason that it was mentioned previously that neglecting a_- was analogous to the rotating wave approximation. It is interesting to note that neglecting the counter-rotating field component of the wave gives rise to the Bloch-Siegert shift [7].

Solving the two-level system for the frequency, ω, results in a splitting in the solution shown below,

$$\omega = \frac{\omega - \omega_0}{2} \pm \frac{1}{2}\sqrt{(\omega - \omega_0)^2 + \frac{|V_{12}|^2}{\hbar^2}} \tag{B.1}$$

where,

$$\omega_r \equiv \frac{1}{2}\sqrt{(\omega - \omega_0)^2 + \frac{|V_{12}|^2}{\hbar^2}} \tag{B.2}$$

is called the Rabi flopping frequency. The splitting in the solution shows how the resonant frequency changes when the coupling between the two levels becomes significant. The power of this relation is that there is no assumption on the strength of the field and does not require perturbation theory. If the applied field has the same frequency as the resonant frequency, eq. (B.2) becomes purely the Rabi flopping

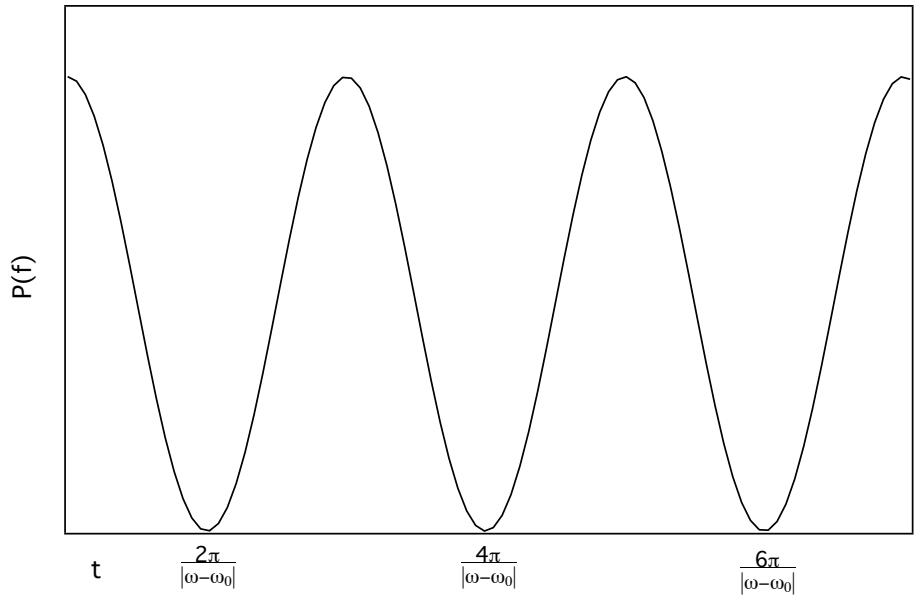

Figure B.1: Time-dependent perturbation theory result for the two-level atomic system. The plot is the probability evolution of being in one of the two states as a function of time [15] with a magnitude of $[|V_{ab}|/(\hbar(\omega_0 - \omega))]^2$.

frequency. It becomes,

$$\omega = \frac{|V_{12}|}{2\hbar} = \frac{\omega_{12}}{2} \tag{B.3}$$

where V_{12} is the strength of the coupling in units of energy and ω_{12} is the strength of the coupling in units of angular frequency. From eq. B.3), the rate that the probability of the particle going from one state to the other is the the Rabi flopping frequency. Although the probability evolution is qualitatively the same as Fig. B.1, they differ in one very important aspect: the probability that the particle is in the initial state becomes *exactly* zero at certain instants when using the RWA. Note that probability of being in upper state is exactly 90° out of phase with the probability of being in the lower state. The reason for this discussion is that the oscillators for wireless energy transfer undergo the same splitting when they are coupled together.

B.2 2-oscillator case - Undriven, Neglecting Losses

To find the resonant frequencies of this system in the absence of any losses and no driving force, eq. (3.4) becomes,

$$\begin{bmatrix} \omega - \omega_1 & -\omega_{12} \\ -\omega_{21} & \omega - \omega_2 \end{bmatrix} \begin{pmatrix} A_1 \\ A_2 \end{pmatrix} = \begin{pmatrix} 0 \\ 0 \end{pmatrix} \tag{B.4}$$

For ω to have a non-trivial solution, the determinant of the coefficient matrix *must* be equal to zero. Taking the determinant results in the following quadratic equation,

$$\omega^2 - (\omega_1 + \omega_2)\omega + \omega_1\omega_2 - \omega_{12}^2 = 0 \tag{B.5}$$

and using the quadratic formula yields the following two roots,

$$\omega = \frac{\omega_1 + \omega_2}{2} \pm \frac{1}{2}\sqrt{(\omega_1 - \omega_2)^2 + 4\omega_{12}^2}. \tag{B.6}$$

This equation is similar to eq. (B.1) where the splitting term is of the same form as the Rabi flopping frequency. Assuming both oscillators are tuned such that their resonant frequencies are the same (ie: $\omega_1 = \omega_2 = \omega_0$) eq. (B.6) simplifies to,

$$\omega = \omega_0 \pm \omega_{12} \tag{B.7}$$

which is of the form expected from the lossless atomic system. What this expression is saying is that the rate that the amplitude (ie: energy) of the oscillators is transferred from the transmitter oscillator to the receiver oscillator is given by the coupling coefficient, ω_{12}.

B.3 2-oscillator case - Undriven, Including Losses

In more realistic systems, losses play a role in the expected result of any system. Therefore, the analysis from the previous section is repeated with the inclusion of the decay rate coefficients, Γ_1 and Γ_2. The system of equations is now,

$$\begin{bmatrix} j(\omega - \omega_1) + \Gamma_1 & -j\omega_{12} \\ -j\omega_{21} & j(\omega - \omega_2) + \Gamma_2 \end{bmatrix} \begin{pmatrix} A_1 \\ A_2 \end{pmatrix} = \begin{pmatrix} 0 \\ 0 \end{pmatrix}. \tag{B.8}$$

The following result for ω is obtained using the same method as the lossless case and assuming that drive and resonant frequencies are equal.

$$\omega = \omega_0 + \frac{j(\Gamma_1 + \Gamma_2)}{2} \pm \frac{1}{2}\sqrt{4\omega_{12}^2 - (\Gamma_1 - \Gamma_2)^2} \tag{B.9}$$

The splitting is obtained again, but is diminished by the addition of the decay rates. There are two important additions to this solution comparing it to eq. (B.7). The first is that there is now an imaginary term equivalent to the average decay rate. This gives rise to an exponential decay of the energy in the system. The second is a condition on ω_{12} for there to be coupling in the system. Closer inspection of the discrimanent yields the following condition for splitting in the system:

$$4\omega_{12}^2 - (\Gamma_1 - \Gamma_2)^2 > 0 \tag{B.10}$$

or,

$$|\omega_{12}| > \frac{|\Gamma_1 - \Gamma_2|}{2} \tag{B.11}$$

This condition illustrates that the coupling coefficient between the oscillators must be greater than any difference in the inherent losses associated with each oscillator. If the coupling coefficient falls below this threshold then the splitting in the resonant frequency disappears and becomes an extra exponential loss factor.

Appendix C

Inductance Formulae

C.1 Motivation

Since describing an accurate model is the primary focus of this work, it is necessary to go over some of the key pieces that make the model of any use at all. Those pieces are the self-inductance and the mutual inductance. This is exemplified by referring to the transfer function for two resonant oscillators,

$$\left|\frac{V_2}{V_1}\right| = Q_2 \frac{M_{12}}{L_1} \tag{C.1}$$

where L_1 is the self-inductance of the transmitting oscillator, M_{12} is the mutual inductance between the transmitting and receiving oscillator, and Q_2 is the quality factor for the receiving oscillator. In this form it can be seen that the transfer function shows that the ratio of the AC voltages on the oscillators is based on the magnetic energy that is transferred to the receiving oscillator (ie: M_{12}) as a fraction of the available magnetic energy (ie: L_1). Since the system is in a regime of strong resonance the process is enhanced through the quality of the resonance (ie: Q_2). The quality factor is difficult to predict exactly due to dependencies of the physical surroundings in the system. Therefore, in order to make the predictions as accurate as possible, the relations for the self-inductance and mutual inductance must be accurate. As it turns out, the mutual inductance is not a straight forward calculation and if the appropriate solution is not chosen without care, there will likely be artifacts in the computed solutions. This appendix is meant to show which equations were used for the calculations in this work and also to illustrate some of the difficulties with accurately determining the mutual inductance.

C.2 Self-Inductance

The geometry of each resonant oscillator has been a circular loop made of a copper pipe. This dramatically simplifies calculating the self-inductance since this is a common geometry found in almost all standard electricity and magnetism textbooks. For a circular loop of radius, r, cross-sectional radius, a, and number of turns, n, the equation for the self-inductance is given by [16],

$$L = n^2 \mu_0 r \left(\ln \frac{8r}{a} - \frac{7}{4} \right). \tag{C.2}$$

Knowing the self-inductance enables calculating the stored energy in the loop through,

$$U = \frac{1}{2}LI^2. \tag{C.3}$$

The current flowing through the loop will tend to be a design criteria and should be known, leading to the stored energy in the loop. It is important to note that the self-inductance is strongly dependent on the number of turns in the loop. Therefore, if needed, the amount of magnetic energy can be dramatically enhanced through additional turns. This can then be converted into the potential maximum power transferred from the loop using $P = \omega U$.

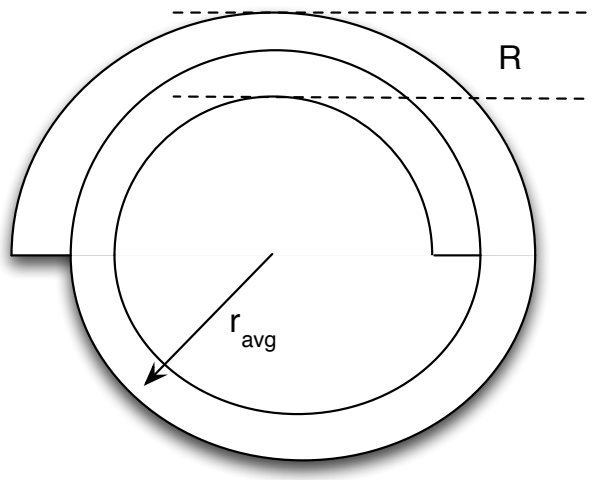

Figure C.1: Example geometry of a flat spiral.

Another useful geometry for wireless energy transfer would be a circular spiral. This geometry maximizes the inductance for a give size of loop while not having to have a potentially long solenoid, as shown by Fig. C.1. This geometry is also useful as it could be placed on a printed circuit board. The inductance is given by Wheeler's formula [17],

$$L = \frac{(Nr_{avg})^2}{8r_{avg} + 11R} \tag{C.4}$$

where N is the number of turns in the spiral, r_{avg} is the average coil radius and R is the coil width (ie: the distance from the centre of the spiral to the outer edge).

C.3 Mutual Inductance

The mutual inductance is similar to the self-inductance as it also depends only on the particular geometry of the system. However, it is more complicated because it

depends on the relative geometry between the two objects in question. With the self-inductance, the system can range from a rectangular slab to a circular loops and as long as its geometry remains constant the self-inductance will also remain constant. Unfortunately the mutual inductance requires more care because the orientation, layout, and physical size are all very important parameters.

The mutual inductance refers to the amount of magnetic flux emitted from one object captured by the physical geometry of a second object. With the case for circular loops, the capturing area for the receiving coil is the area enclosed by the loop. In equation form, the mutual inductance is expressed as:

$$M_{ps} = I_p \iint \bar{B}_p \cdot d\bar{S}_s \tag{C.5}$$

where M is the mutual inductance, I_p is the current in the primary loop, B_p is the magnetic field of the primary loop, and S_s is the area mapped out by the secondary loop. Since the mutual inductance depends on the relative geometry of the objects in question, it is not difficult to imagine evaluating eq. (C.5) analytically is extremely difficult or even impossible. When complicated geometries are required numerical techniques such as Finite Element Method or manually integrating the magnetic field through the loop. There is some solace in the fact that there are some simple geometries that have exact solutions that can be used as baselines for numerical code to compare against. The mutual inductance can also be expressed as infinite series solutions, with an appropriate interior and exterior solution[18]. However, care must be taken to ensure that these series solutions are used in regions where they yield meaningful results. Unfortunately, they do not always have valid results for all space and geometries that may exist for the system.

The mutual inductance is the quantity that links two magnetic objects together. Based on the relative geometry of the two objects, it is not surprising that which object is the primary and which is the secondary object: implying that $M_{ps} = M_{sp}$. This can be seen by manipulating eq. (C.5) into the following form,

$$M_{ps} = \frac{\mu}{4\pi} \oint \oint \frac{dl_p \cdot dl_s}{r_{ps}} = M_{sp}. \tag{C.6}$$

Based purely on the geometry and $dl_p \cdot dl_s$ yielding the same result regardless of the order illustrates that the labeling of which object is the primary and secondary is not important from a theoretical standpoint. It can also be seen from an energy standpoint since the stored mutual energy is given by,

$$U_{mutual} = M_{ps} I_p I_s. \tag{C.7}$$

If $M_{ps} \neq M_{sp}$ then the mutual energy between the two objects would be different based on an arbitrary choice of the primary object. This is not physically realistic and cannot be true, justifying the statement that $M_{ps} = M_{sp}$.

As will be shown in the following sections, for two circular loops, the choice of the primary loop is important from purely a mathematical point of view. All

the solutions discussed require the primary loop to be greater than or equal to the secondary loop. Based on the above discussion, this is a trivial detail with the choice of the primary object is irrelevant in the physical system.

The analysis done in this thesis used two coplanar circular loops of identical radii; however, these solutions have no such restriction on the radii of the loops used. It is with this in mind that the following solutions will be as general as possible. Three solutions to the mutual inductance will be given below. The first will be the standard coaxially aligned coplanar circular loops. The second will be the series solution for coplanar circular loops that are not restricted to the axis. The final solution will be a general solution for arbitrary geometry for two circular loops. All of the theoretical calculations used the third solution.

C.3.1 Coaxially Aligned Coplanar Circular Loops

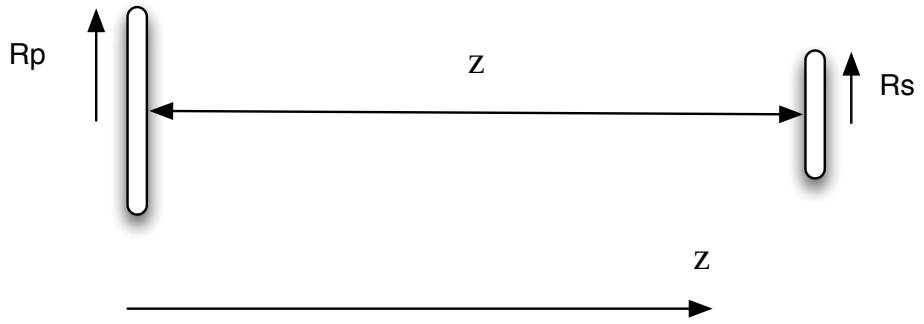

Figure C.2: Schematic of two circular loops coaxially aligned with differing radii.

The solution to the first geometry was originally derived by Maxwell [19]. Consider two coils of differing radii, R_p and R_s, separated by a distance z along a common axis as shown in Fig. C.2. Evaluation of the mutual inductance yields,

$$M = \frac{2\mu}{k}\sqrt{R_p R_s}\left[\left(1 - \frac{k^2}{2}\right)K(k) - E(k)\right] \tag{C.8}$$

where μ is the permeability of the medium, $K(k)$ and $E(k)$ are the complete elliptic integrals of the first and second kind, and k is the input parameter required for $K(k)$ and $E(k)$. The parameter k is a function of the radii of the loops and their separation and is expressed as,

$$k^2 = \frac{4R_p R_s}{(R_p + R_s)^2 + z^2}. \tag{C.9}$$

The only restriction for this equation is that the radius of the primary loop must be greater than or equal the radius of the secondary loop ($R_p > R_s$). However, this complication can be avoided by switching which loop is the primary and which is

the secondary before performing the calculation.

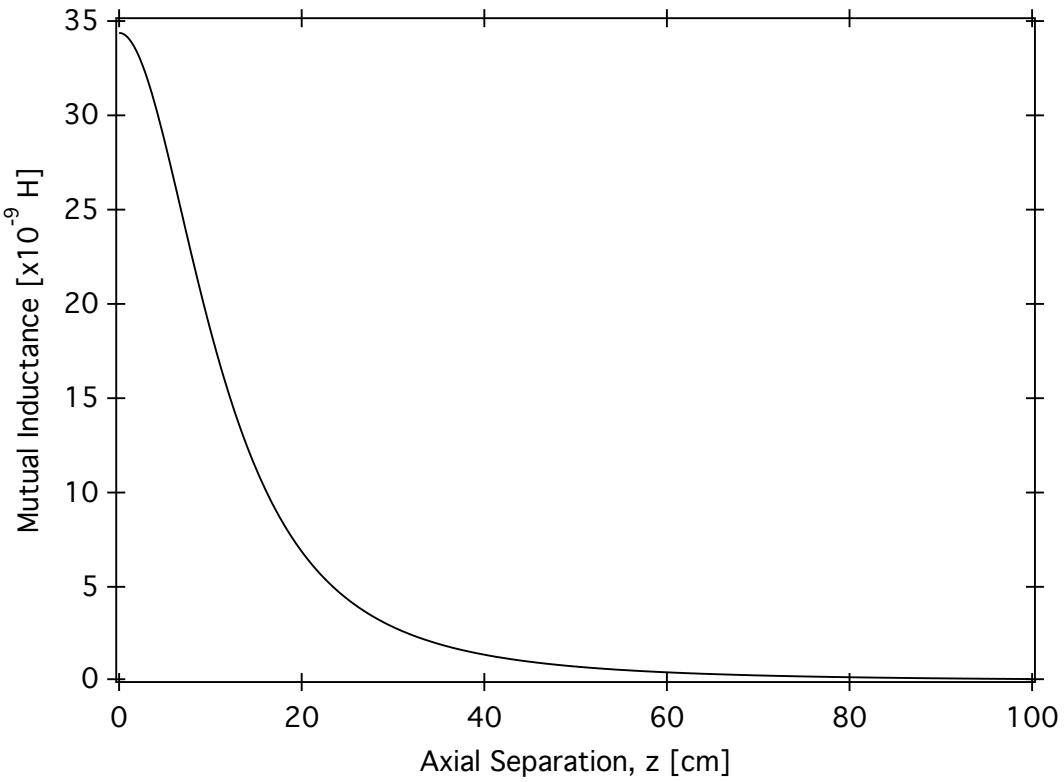

Figure C.3: Mutual inductance of two circular loops aligned coaxially with the primary loop radius of 15 cm and secondary loop radius of 5 cm.

A plot of eq. (C.8) with a primary radius of 15 cm and a secondary radius of 5 cm is shown in Fig. C.3. As it illustrates, the mutual inductance is at a maximum when the two loops are effectively touching each other and then rapidly decays as the separation distance is increased. This clearly illustrates why many devices that rely on the mutual inductance (ie: transformers) are setup to have the primary and secondary objects as close as possible.

C.3.2 Coplanar Circular Loops - Series Solution

The next solution considered is the series solution given by Snow [18]. This solution is more general than the coaxial solution discussed in the previous section with the secondary coil not restricted to the same axis as the primary coil. However, the loops must still remain coplanar. Series solutions are generally very useful because they have the ability to yield results for systems that may not have an analytical solution. They also tend to be computationally very fast.

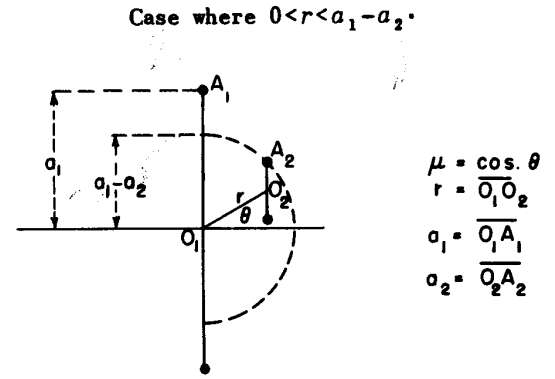

(a) Interior

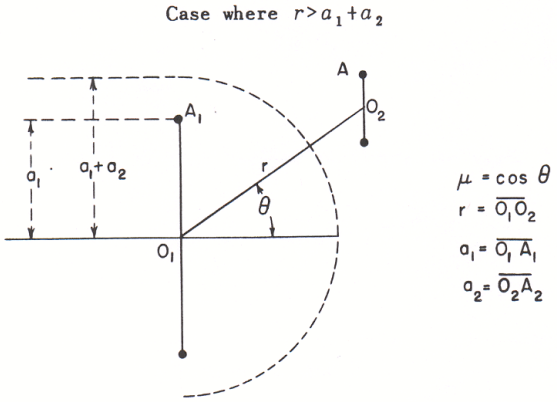

(b) Exterior

Figure C.4: Geometry for the different series solutions from Snow [18]. The images are taken from Snow's handbook.

Series solutions have separate forms depending on spacial orientation of the system at a given instant: the interior solution and the exterior solution. Where the interior and exterior solutions are valid are based on the geometry. Fig. (C.4) illustrates where the interior and exterior solutions exist for two coplanar loops and defines some symbols used in the two solutions. The solution for the mutual inductance given as interior and exterior solutions is given respectively by [18],

$$M = \frac{4\pi^{\frac{3}{2}}a_2^2}{a_1}\sum_{n=0}^{\infty}(-1)^n\left(\frac{r}{a_1}\right)^{2n}\frac{\Gamma(n+\frac{3}{2})}{n!}F_nP_{2n}(\mu) \tag{C.10}$$

where F_n is the hypergeometric series and is expressed with $F_n = F\left(n+\frac{1}{2}, n+\frac{3}{2}, 2; \frac{a_2^2}{a_1^2}\right)$

and,

$$M = \frac{4\pi^{\frac{3}{2}} a_2^2}{a_1} \sum_{n=1}^{\infty} (-1)^{n+1} \left(\frac{a_1}{r}\right)^{2n+1} \frac{\Gamma(n+\frac{1}{2})}{(n-1)!} F_n P_{2n}(\mu) \tag{C.11}$$

with $F_n = F\left(-n, 1-n, 2; \frac{a_2^2}{a_1^2}\right)$.

Unfortunately, there is a problem with some geometries of physically realistic systems. Babic *et al* [20] also discuss that there are also problems with convergence in certain instances. Closer inspection of the regions for the interior and exterior solutions yield the problem. The interior solution exists when the distance between the primary and secondary loops is $0 < r < a_1 - a_2$ and the exterior solution exists when $r > a_1 + a_2$. Consider the following geometry: two circular loops with the primary loop having a radius of 15 cm and the radius of the secondary loop is 5 cm. With this system, the interior solution exists from $0 < r < 10$ cm and the exterior solution exists for $r > 20$ cm. There is a gap of 10 cm where there is no solution for the mutual inductance! This is obviously an unphysical manifestation of this particular solution. The two loops would not cease to have a defined mutual interaction for a particular region of space. In the case for two identically sized loops, the interior solution ceases to exist at all!

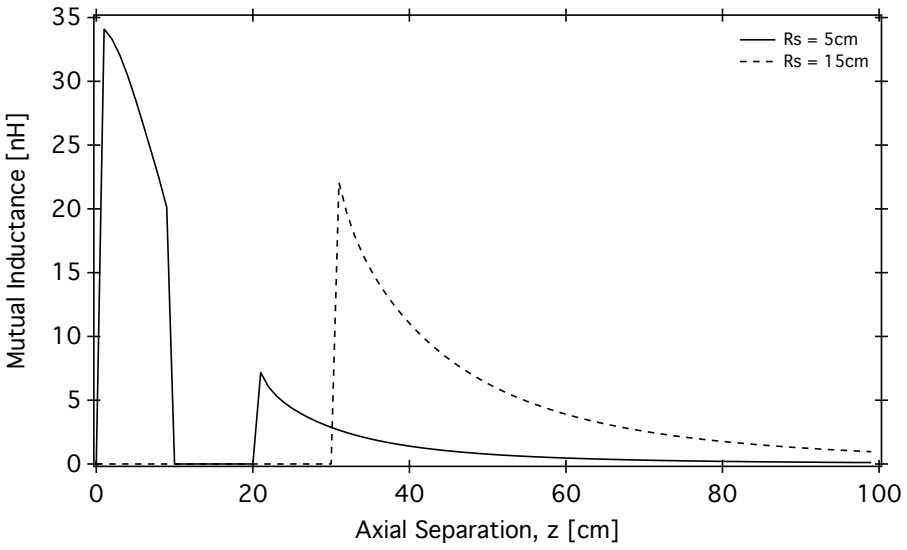

Figure C.5: Mutual inductance of two circular loops aligned coaxially using the series solution.

Fig. C.5 illustrates the unphysical nature of the solutions with the distance gap between the two solutions and also the lack of an interior solution for identically sized loops. However, the solution is not without merit. If the radius of the secondary loop is much smaller than the radius of the primary loop then the problem is as severe.

Although originally an attractive possibility for quickly determining the mutual

inductance for coplanar loops, it is not possible to obtain physically accurate values for the geometries used in this thesis.

C.3.3 Two Circular Loops - Arbitrary Geometry

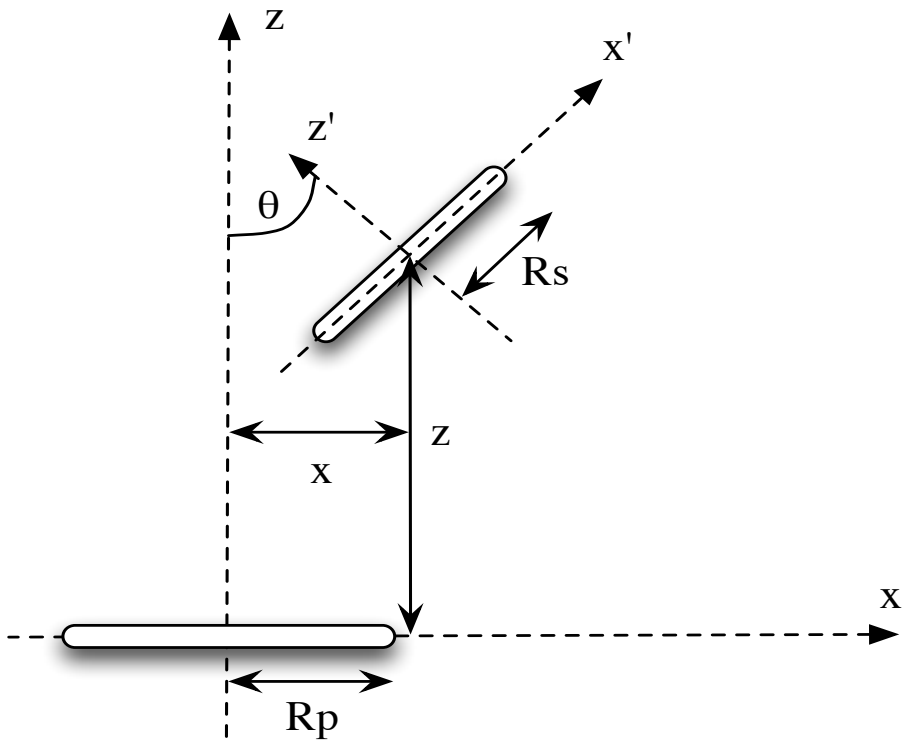

Figure C.6: Schematic of two circular loops with the receiver at an arbitrary relative orientation with different radii for each loop.

The final solution presented is the solution utilized in this thesis. It is the most general of the solutions presented. Like the previous solutions, this solution requires the primary loop to be greater than or equal to the radius of the secondary loop; which can easily be dealt with by changing the which loop is the primary before computation. Fig. C.6 shows a two loop system with the most general geometry the solution can handle and Fig. C.7 shows a similar system with only a lateral misalignment. The only requirement to use the solution is the z and z' axes must be in the same plane.

This solution presented was originally proposed by Grover [21] and then confirmed by Babic *et al* [20, 22] where any configuration can be calculated. The solution for the mutual inductance is given by,

$$M = \frac{2\mu_0}{\pi}\sqrt{R_p R_s}\int_0^{\pi} \frac{(\cos\theta - \frac{d}{R_s}\cos\phi)\Psi(k)}{k\sqrt{V^3}}d\phi \tag{C.12}$$

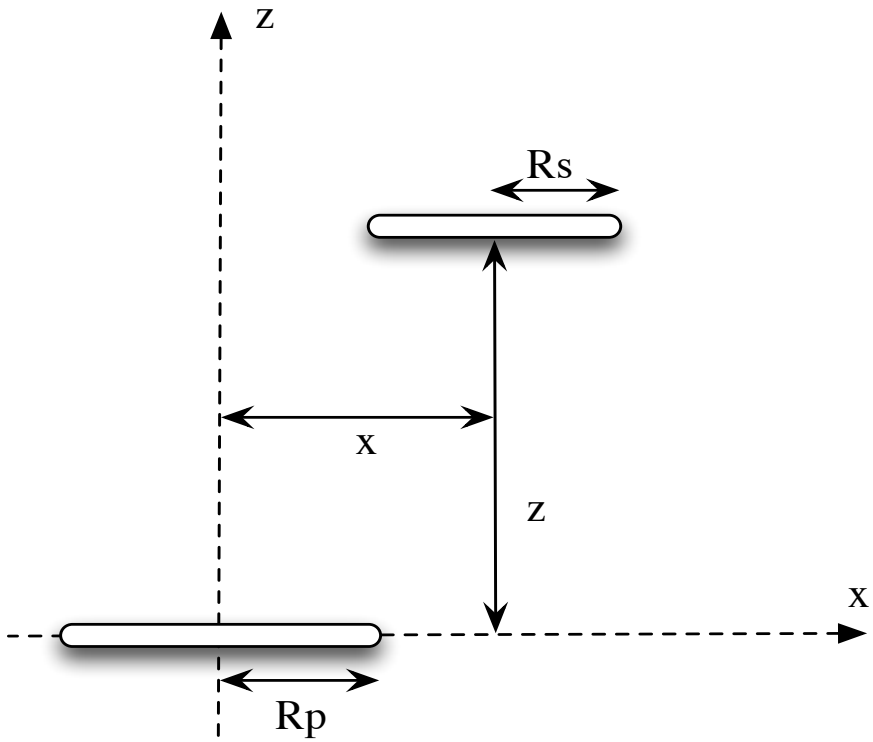

Figure C.7: Schematic of two circular loops with no angular differentiation with different radii for each loop.

where all the variables used are given by

$$\alpha = \frac{R_s}{R_p},\ \beta = \frac{z}{R_p},$$

$$V = \sqrt{1 - \cos^2\phi \sin^2\theta - 2\frac{x}{R_s}\cos\phi\cos\theta + \frac{x^2}{R_s^2}},$$

$$k^2 = \frac{4\alpha V}{(1+\alpha V)^2 + \xi^2},\ \xi = \beta - \alpha\cos\phi\sin\theta,$$

$$\text{and } \Psi(k) = \left(1 - \frac{k^2}{2}\right)K(k) - E(k).$$

The solution itself is a generalization of the coaxially aligned solution. If the two loops are coplanar and coaxially aligned, $\theta = 0$ and $x = 0$, then eq. C.12 reduces to eq. C.8.

Many of the systems in this work were constrained to coplanar loops, $\theta = 0$, which considerably simplifies eq. (C.12). Even with these simplifications, eq. (C.12) remains an incredibly difficult expression to evaluate analytically. Numerical techniques were used in order to make evaluation of the expression tractable. As an

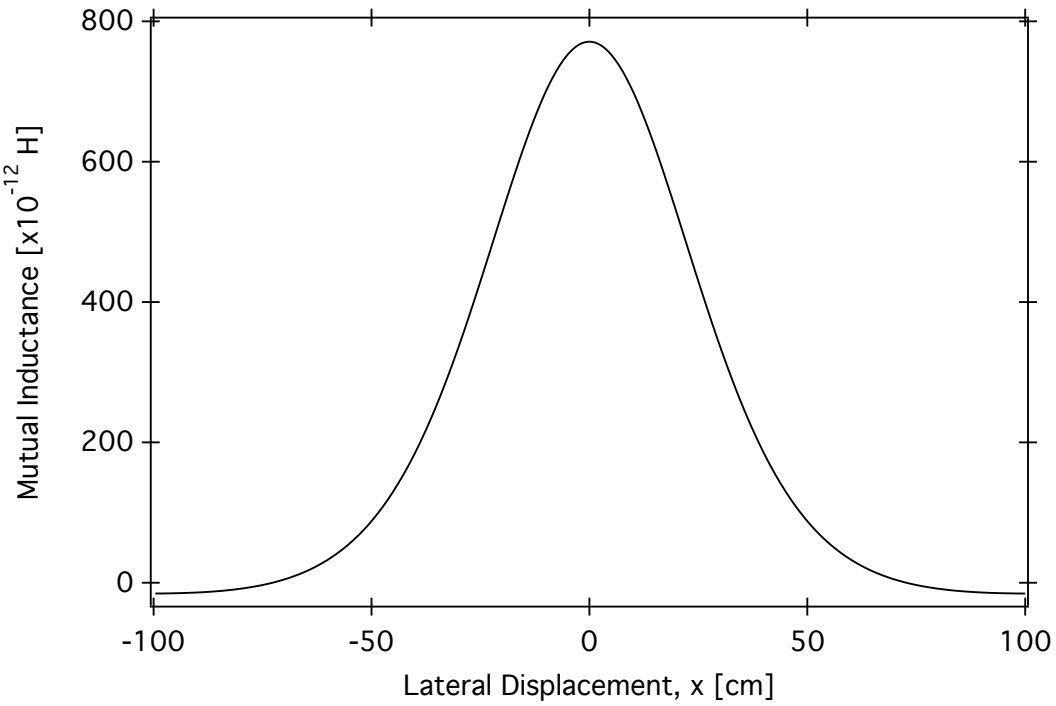

Figure C.8: Lateral scan of the mutual inductance of two coplanar circular loops with the primary loop radius of 15 cm and secondary loop radius of 5 cm.

example, Fig. C.8 shows a plot where the secondary loop is scanned laterally. The shape of the curve makes intuitive sense when in comparison to the axial plot in Fig. C.3. Given how quickly the mutual inductance decays with distance, the quick decay with lateral misalignments is to be expected.

It is interesting to note that even though calculations for the mutual inductance have been known for a very long time, only the simplest of geometries have solutions. The benchmark was set by Grover [23, 21] who had compiled a large set of calculations for many relevant non-trivial geometries with a good degree of accuracy. However, the subject still is still active with an article by Kim *et al* [24] who derived a new expression for two coplanar loops with lateral misalignment. However, their result did not match the results from Grover. Recently, different groups have looked into the problem [20, 22, 25] and their results confirm Grover's expression.